ANALYSIS OF CHITOSAN BINDER-BASED ZNO PHOTOANODE FOR DYE-SENSITIZED SOLAR CELL

KHAIRUL HAREEQ HAIQAL BIN KHAIRUL AZMAN

UNIVERSITI TEKNIKAL MALAYSIA MELAKA

ANALYSIS OF CHITOSAN BINDER-BASED ZNO PHOTOANODE FOR DYE-SENSITIZED SOLAR CELL

KHAIRUL HAREEQ HAIQAL BIN KHAIRUL AZMAN

This report is submitted in partial fulfilment of the requirements for the degree of Bachelor of Electronic Engineering with Honours

Faculty of Electronic and Computer Engineering
Universiti Teknikal Malaysia Melaka

2021

DECLARATION

I declare that this report entitled "ANALYSIS OF CHITOSAN BINDER-BASED ZnO PHOTOANODE FOR DYE-SENSITIZED SOLAR CELL" is the result of my own work except for quotes as cited in the references.

Signature :

Author : KHAIRUL HAREEQ HAIQAL BIN KHAIRUL AZMAN

Date : 4 AUGUST 2021

APPROVAL

I hereby declare that I have read this thesis and in my opinion this thesis is sufficient in terms of scope and quality for the award of Bachelor of Electronic Engineering with Honours.

Signature : _____

Supervisor Name : Dr. Mohamad Harris bin Misran

Date : 4/8/2021

DEDICATION

I dedicate this whole thesis to my family as it has supported me through many things during completing this thesis and they have always been with me at my up and down. I also dedicated this thesis to my supervisor who taught me that mastering is not a priority, but diligence and passion are the key pillars in completing a project.

ABSTRACT

Dye-Sensitized Solar Cell (DSSC) have been attracting huge attention because of their efficiency, simple and low-cost fabrication process. In comparison to a commercially available silicon solar cell, DSSC can be produced at a lower cost per generated power [1]. This project will use chitosan as a binder to the ZnO photoanode to analyse the performance of dye-sensitized solar cell. The chitosan has been prepared by four different techniques. The obtained chitosan was characterized using scanning electron microscopy (SEM), Fourier transform infrared spectroscopy (FTIR), and X-ray diffraction (XRD). Samples of white powder chitosan with degree of deacetylation of 78% were obtained, as determined by FTIR spectra. The similar chitosan was used to fabricate a dye-sensitized solar cell using 6% of chitosan and achieving voltage value of 0.2783V and current value of 0.2519A. A simulation using GPVDM software were done by varying the thickness of chitosan and manage to obtain the highest efficiency of 2.7645% with 160nm thickness layer of chitosan .

ABSTRAK

Dye-Sensitized Solar Cell (DSSC) telah menarik perhatian yang besar kerana kecekapan mereka, proses fabrikasi yang mudah dan kos yang rendah. Sebagai perbandingan dengan sel solar silikon yang ada secara komersial, DSSC dapat dihasilkan dengan kos yang lebih rendah per kuasa yang dihasilkan. Projek ini akan menggunakan kitosan sebagai pengikat kepada fotoanod ZnO untuk analisis prestasi sel solar yang peka dengan pewarna. Kitosan telah disediakan dengan empat teknik yang berbeza. Kitosan yang diperoleh dicirikan menggunakan mikroskopi elektron imbasan (SEM), spektroskopi inframerah transformasi Fourier (FTIR), dan difraksi sinar-X (XRD). Sampel kitosan serbuk putih dengan tahap deasetilasi 78% diperolehi, seperti yang ditetapkan oleh spektrum FTIR. Kitosan yang sama digunakan untuk membuat sel solar peka pewarna menggunakan 6% kitosan dan nilai voltan 0.2783V dan nilai semasa 0.2519A dicapai. Simulasi menggunakan perisian GPVDM dilakukan dengan mengubah ketebalan kitosan dan berjaya mendapatkan kecekapan tertinggi 2,7645% dengan lapisan kitosan ketebalan 160nm.

ACKNOWLEDGEMENTS

First of all, I am thankful and grateful to ALLAH S.W.T for providing me with everything that I required in completing this project. I have taken efforts in this project. However, this project would not have been possible to achieve its objectives without the kind support and help of many individuals. I would like to extend my sincere thanks to all of them.

Next, I would like to express my sincere and deepest thanks to my research guide and supervisor, Dr. Mohamad Harris bin Misran and co supervisor Dr. Muhammad Idzdihar bin Idris who has guided me at every stage of my research work and constantly encourage me during completing this project.

Next, I wish thanks to the lecturers and staff from the Faculty of Electronics and Computer Engineering, and Faculty of Manufacturing Engineering for their encouragement and guidance during my research to complete this final year project.

Last but not least, very special thanks to my family and friends for their spiritual support and kind cooperation for the report completion, from beginning till the end.

TABLE OF CONTENTS

LIST OF FIGURES

LIST OF TABLES

LIST OF SYMBOLS AND ABBREVIATIONS

DSSCs	:	Dye-Sensitized Solar Cells
ZnO	:	Zinc Oxide
V	:	Voltage
A	:	Ampere
ITO	:	Indium Tin Oxide
PV	:	Photovoltaic
CIGS	:	Copper Indium Gallium Selenide
CdTe	:	Cadmium Telluride
GO	:	Graphene Oxide
TiO2	:	Titanium Dioxide
HCl	:	Hydrochloric Acid
NaOH	:	Sodium Hydroxide
XRD	:	X-ray Diffraction Spectroscopy
SEM	:	Scanning Electron Microscope
FTIR	:	Fourier-transform Infrared Spectroscopy
UV-Vis	:	Ultraviolet-visible Spectroscopy

CHAPTER 1

INTRODUCTION

1.1 Project Background

Dye-Sensitized Solar Cell (DSSC) is advancing today as one of the reassuring third-generation solar cells. To distinguish the purpose of light absorption from the charge carrier's transport, the DSSC varies from traditional semiconductor devices. The dye sensitizer will absorb the incident light, and the electron transfer reaction will happen due to the light energy. DSSC's efficiency can be intensified by altering or adjusting the parameter used for the solar cell. The critical problems with the current DSSC development were the efficiency of low rate solar-electricity conversion. This project aims to produce dye-sensitized solar cells and evaluate the ZnO photoanode solar cell-based chitosan binder's efficiency. ZnO photoanode have a higher location

in the conduction band, allowing greater photovoltage to be produced. However, with the addition of chitosan-based, its efficiency is likely to increase further, allowing more electrodes to bind to the DSSC photoanode. The synthesis of ZnO photoanode in this study can be carried out by several test synthesis of nanoparticles to study and identify ZnO growth. Chitosan-based synthesis can be carried out according to the recipe that other researchers have produced. The experiment's output can be analyzed using several methods and observed the samples' visual images. There are essential steps in paste preparation, glass deposition, stain with dye, counter electrode preparation, solar cell assembly, and performance analysis for the DSSC manufacturing portion. Therefore, the methodology for this analysis is based on the Design of Experiment (DOE) to link the flow process to the outputs obtained.

1.2 Problem Statement

Over the past 20 years, DSSC's efficiency has continued to rise, with a confirmed 14.1% record reached by Professor Michael Graetzel, a G24 Power Consultative Council Member, and his team. Even so, there are still multiple research have been conducted to further increase the efficiency of DSSC so one day it can replace conventional solar cell. Polymer coatings make metal more flexible and durable. There are many polymer/metal pairing in use throughout a variety of industries and application. Chitosan is a polysaccharide composed mainly of β-(1,4)-linked 2-deoxy-2-amino-D-glucopyranose units. It was considered an environment-friendly binder, possesses good viscosity and an effective electron binder. But can polymer chitosan improve the efficiency of dye-sensitized solar cell if use as an electrode binder?

1.3 Objectives

There are a few objectives that need to be achieved in this project. The objectives of this project are listed below:

i. To synthesize, characterize and analyze Chitosan from shrimp shell

ii. To analyze the amount of Chitosan with the efficiency of solar cell

iii. To analyze performance of fully fabricated DSSC utilizing Chitosan as the photoanode binder.

1.4 Scope of Work

The focus of this study will revolve around the understanding of Dye-Sensitized Solar Cell's layer, principle, and properties. The fabrication of solar cell using Chitosan as the ZnO photoanode binder on Indium Tin Oxide (ITO) will be deployed. The synthesis of chitosan will use shrimp shell as the based material. This research focuses on the developing and analyze ZnO photoanode with different amount of Chitosan that act as a binder of the DSSC based on its structure, characteristic, electrical properties, and energy conversion efficiency.

1.5 Thesis Structure

In this thesis, there will be five chapters to describe the project flow which is fabrication of Chitosan binder-based ZnO Photoanode for Dye-Sensitized Solar Cell. The chapters in the thesis will be as follows: Introduction, Literature Review, Methodology, Result, Discussion, and Conclusion.

Chapter 1 - This chapter discussed the background of the study, problem statement, objectives, and scope of work of the project.

Chapter 2 – This chapter consists of the background study and research about this project before fabrication. Besides, the background study contains the fundamental of the dye-sensitized solar cell and previous works and journals that related to this project.

Chapter 3 – This chapter involved the process employed during the project development in methodology part, including the equipment, materials used and fabrication procedures for the dye-sensitized solar cell.

Chapter 4 – This chapter will explain detail about the result and discussion as well as analysis of the project after the fabrication process is done. Moreover, the electrical characteristic of dye-sensitized solar cell and calculation of the efficiency will also be defined.

Chapter 5 – This is the last chapter which is the conclusion of this project. The conclusion consists of the summary and recommendation for a better future development of this project.

CHAPTER 2

BACKGROUND STUDY

Background Study chapter contains the previous works on the experimental result and density fundamental theory applied in this project. It contains the information accumulation of the project in order to complete the whole project.

2.1 Solar Cell

A solar cell is a semi-conductor system that by electromechanical reaction converts incident light from sunlight into electrical energy (photovoltaic effect) [1]. Solar cells are similarly produced and stored as computer memory chips [2]. The French scientist Edmond Becquerel first demonstrated the photovoltaic effect in 1839. Later, by developing selenium semiconductor with a gold electrode thin film, Charles Fritts made the first photovoltaic cell in 1883[1]. While promising, photovoltaic cells are faced with less efficiency and high-cost production, which refrain from large-scale

use. Many attempts have been made to improve photovoltaic cells' efficiency to regulate electricity prices [3].

2.1.1 Generation of solar cell

Solar energy can either be obtained directly from sunlight or by indirect methods. Various technologies for harvesting solar energy have been developed, such as solar cells, which are efficient and have a strong market demand [2]. Based on solar cell's relative cost and efficacy, they are typically divided into three distinct groups. Inverse to single and multi-crystalline solar silicone cells is the first generation of PM technology. As a thin film, the second generation of PV was launched, reducing the cost. Double joints, triple junctions and nanotechnology are integrated into solar cell production methods in the third generation [3].

Table 2.1: Generation of solar cell [1]

Generation of Solar Cells		
First Generation	Second Generation	Third Generation
- Monocrystalline (Mono c-Si) - Polycrystalline (Poly c-Si) - Amorphous Silicon Cells - Hybrid Silicon	- Amorphous Silicon (a-Si) - Cadmium Telluride (Cd-Te) - Copper-Indium-Selenide (CIS) - Copper-Indium-Gallium-Diselenide (CIGS)	- Dye-Sensitized (DSSC) - Perovskite (cell) - Organic (OPV) - Quantum Dot (QD) - Kesterite solar cell

2.1.1.1 First generation solar cell

The solar cells of the first generation are placed on the most powerful and wholesale feasible silicon [4]. Bell Laboratories formed the first solar silicon cell in 1954, with an efficiency of 6 %. Conventional silicon solar cells, which are currently

the most competent solar cells available for residential use and registered for about 80% of all solar panels sold worldwide, are the first commercial silicon. In terms of single-cell photovoltaic materials, silicon solar cells are the most effective, and silicon is the largest element on earth. It is a semiconductor material suitable for PV applications with an energy band gap of 1.1eV [1]. For PV applications with magnificent properties (such as non-toxic, affluence, durable performance, etc.) and good manufacturing, Silicon has been an enticing alternative [6]. Silicon supply is the limited disadvantage of solar cells, requiring expensive processing technology and wasting higher energy photons like heat [2]. First-generation solar cells consist of monocrystalline, polycrystalline, amorphous, and hybrid silicon solar cells [4]. Monocrystalline silicon solar cells are formed by a single crystal of silicon cultivated under highly composed conditions. These PV can perform up to 24 percent photoconversion capacity, but their cost of production and poor conduct at exalted temperatures are the fundamental problems. By growing distant intertwine silicon crystals after monocrystalline, polycrystalline silicon solar cells are formed, making them less costly and easier to prepare than monocrystalline. The efficiency of photoconversion over the construction amount is, however, sacrificed. Solar cells of the first generation are amorphous solar silicon cells which generate energy at a minimum extent, for a compact and self-powered electronic equipment. Silicon's thin film is applied on metallic, plastic substrates, or glass in amorphous silicon solar cells, differ from monocrystalline and polycrystalline solar cells. Because of the thin film, the solar cell is greatly malleable, unfortunately its performance was lower (10 percent) and at low-light intensities, it does not work. For the purpose of combining the benefits of amorphous and crystalline silicon, hybrid silicon solar cells were designed. This type of solar cell, amorphous silicon is place over a crystalline silicon

wafer. The hybrid solar cell's photoconversion efficiency in dispersed light is more significant contrast to its predecessors. In addition, the act also increased at exalted temperatures compensate to amorphous silicon [4].

2.1.1.2 Second generation solar cell

Second-generation solar cells are based on thin-film. The architecture of the solar cell is layered plus the usage volume of element is smaller than that of solar crystalline silicon cells [4]. Thin-film solar cells consist of successive thin layers of solar cells deposited just 1 to 4 μm thick on a large, low-cost substrate such as glass, polymer, or metal. Thin films can be packed into compact and lightweight structures which can be easily incorporated into building components (building-integrated PV, BIPV) [5]. Manufacturing costs are also much smaller, leading to the highly economical production of solar cells [4]. Thin film solar cells start to be deployed in large quantities after more than 20 years of R&D. In theory, thin film solar cells can supply less electricity than c-Si wafer solar cells [1]. Thin-film solar cells are based on amorphous silicon (a-Si), Copper Indium Gallium Selenide (CIGS), Cadmium Telluride (CdTe), and Copper Indium Selenide (CIS) and belong to the second generation [2]. 24.7 percent of the peak efficiency was achieved for a thin-film solar cell [4]. Higher yields (in terms of installed kWh/KWp) and shorter payback time for electricity are considered for CIGS solar cells. CdTe solar cells, by comparison, actually share the most important portion of thin films commercially. It is a leading candidate for the stability, high absorbability, and variability of production methods in the thin-film arena [6]. The thin-film cells' highest efficiency is 21.6 percent for CIGS cells, 21.4 percent for CdTe cells, and 11.8 percent for amorphous silicon. Even though these thin-film solar cells have lower costs and better efficiency, they do have some imperfections. Some of the substance which produces this cell is either limited

and overpriced (indium) or highly toxic (cadmium) [5]. A few significant differences exist between the second-generation solar cells and the first-generation solar cells. The principal distinction from indirect silicon bandgap is the fact that a direct bandgap exists between the semiconductor material used in the cell, but the cells still depend on the p-n junction configuration. There is a top layer of thin-film cells called the winder layer, consisting of a large band gap that swallow more incredible light photons. A lower layer known as the absorber layer is created from a material with a lower bandgap that absorbs a photon of lower energy that is not diffused by the window layer. Its architecture makes it possible to achieve intrinsically better effectiveness [5]. It could take a longer time to solve the production issues and take the cost of production together with the other well-known manufacturers of solar panels. These affects have inspired a new gens of solar cells [5].

2.1.1.3 Third generation solar cell

Third-generation solar cells are the latest solar cell technology. Large-scale studies are devoted in developing third-generation solar cells. The used of advanced nanomaterials akin as graphene nanowires, nanotubes, silicon materials, organic dyes, plus polymer conduction, this study focuses on improving performance [3]. A new generation of solar cells has developed because of the high cost of solar cells from first generation and the toxicity and the lack of materials for second-generation solar cells [5]. The third-generation solar cells are essentially different from the two last generations because they are not dependent on the P-N connector architecture of the other generations. The solar cells of the third generation include solar cells from Organic, Dye-Sensitized, Quantum Dot (QD), Perovskite and Kesterite [6]. The availability of a wide variety of non-toxic and inexpensive products and ease of manufacturing is the impetus behind considering organic cell technology. The active

layer of organic solar cells is made up of donor and acceptor materials that are used for charge separation and transport [5]. In recent years, their performance has been attributed to many substantial changes contributing to greater efficiencies. For commercial systems, OPV module performance are now in the range of 8 percent to 10 percent. For organic cell production, the methods used were high-speed and low-temperature roll-to-roll processing procedures and standard printing [5]. Dye-Sensitized solar cells use dyes that are less complex procedure and do not crave complex PV equipment [6]. Because of their high efficiency, inexpensive, non-complex production processes, environment friendly, clarity, and good flexibility. Dye-sensitized solar cells display improvement from other photovoltaic devices among different solar cells. Although DSSCs performance are good under closed conditions compare to other solar cells, parameters such as efficiency, durability, and expenditure actuate their market applications. The principal components of traditional DSSCs are nanocrystalline semiconductors, sensitizers, redox electrolytes, and counter electrodes [5]. The efficiency of the cells relies on the semiconductor electrode of the dye molecule and the sensitizer. The more sensitive type of dye to the sun will trap more light energy, thereby producing a higher output voltage [4]. By the phenomenon known as the development of multiple excitons, QD Solar cells tend to beat the Shockley-Queisser limit (MEG). QD allows the absorption point in the visible IR regions of the spectrum to occur [6]. Perovskite solar cells are derived from dye-sensitized solar cells. As first discovered in 2009, the adsorption of methylammonium lead halide perovskite on a nanocrystalline TiO2 surface generates a photocurrent with a power conversion efficiency (PCE) of around 3-4 percent in a liquid-based dye-sensitized solar cell structure [5]. Kesterite-based solar cells shine among other thin-film due to their high coefficient of absorption (104 cm -1), possess lesser toxic and

earth-rich components with an average analytical efficiency of about 32 percent. Other advantages of Kesterite material are its isoelectronic to methods of chalcopyrite. It is also an outstanding Indium replacement absorber containing [6].

2.1.2 The efficiency of solar cell

One of the limiting factors in solar cell engineering is the efficacy of solar cells. There will be new data on the efficiency of solar cells per year. . The most crucial requirement for including the results in the tables is that they have been individually measured by an authorized test center, which is mentioned elsewhere. *Table 2.2* summarizes the detail measurements for 'one-sun' (non-concentrator) single-junction cells and submodules [6].

Table 2.2: Proven efficiencies of single-junction terrestrial cells and submodules estimated at 25 ° C under the global AM1.5 spectrum (1000 W/m2) [2]

Classification		Efficiency. %	Area, cm^2	V_{oc}, V	J_{sc}, mA/cm^2	Fill factor, %
Silicon	Si (crystalline cell)	26.7 ± 0.5	79.0 (da)	0.738	42.65	84.9
	Si (multicrystalline cell)	22.3 ± 0.4	3.923 (ap)	0.6742	41.08	80.5
	Si (thin transfer submodule)	21.2 ± 0.4	239.7 (ap)	0.687	38.50	80.3
	Si (thin film minimodule)	10.5 ± 0.3	94.0 (ap)	0.492	29.7	72.1
III-V cells	GaAs (thin film cell)	29.1 ± 0.6	0.998 (ap)	1.1272	29.78	86.7
	GaAs (multicrystalline)	18.4 ± 0.5	4.011 (t)	0.994	23.2	79.7
	InP (crystalline cell)	24.2 ± 0.5	1.008 (ap)	0.939	31.15	82.6
Thin film chalcogenide	CIGS (cell) (Cd-free)	23.35 ± 0.5	1.043 (da)	0.734	39.58	80.4
	CdTe (cell)	21.0 ± 0.4	1.0623(ap)	0.8759	30.25	79.4
	CZTSSe (cell)	11.3 ± 0.3	1.1761(da)	0.5333	33.57	63.0
	CZTS (cell)	10.0 ± 0.2	1.113 (da)	0.7083	21.77	65.1

Amorphous/ Microcrystalline	Si (amorphous cell)	10.2 ± 0.3	1.001 (da)	0.896	16.36	69.8
	Si (microcrystalline cell)	11.9 ± 0.3	1.044 (da)	0.550	29.72	75.0
Perovskite	Perovskite (cell)	20.9 ± 0.7	0.991 (da)	1.125	24.92	74.5
	Perovskite (minimodule)	17.25 ± 0.6	17.277(da)	1.070	20.66	78.1
	Perovskite (submodule)	11.7 ± 0.4	703 (da)	1.073	14.36	75.8
Dye-sensitized	Dye (cell)	11.9 ± 0.4	1.005 (da)	0.744	22.47	71.2
	Dye (minimodule)	10.7 ± 0.4	26.55 (da)	0.754	20.19	69.9
	Dye (submodule)	8.8 ± 0.3	398.8 (da)	0.697	18.42	68.7
Organic	Organic (cell)	11.2 ± 0.3	0.992 (da)	0.780	19.30	74.2
	Organic (minimodule)	9.7 ± 0.3	26.14 (da)	0.806	16.47	73.2

2.2 Dye-sensitized solar cell

Adding a TiO2 nanocrystalline material as the photoanode, O'Regan, and Grätzel introduced the first DSSC in 1991 [3]. Several studies that consider DSSC as one of an efficient, low-cost alternative to conventional solar cells have been published following Grätzel's important and novel contribution to dye-sensitized solar cells (DSSCs) [7]. One of the most up-and-coming photovoltaic technologies is dye-sensitized solar cells (DSSCs) because they generally consist of cheap components and have a simple structure [8]. Dye-sensitized solar cells (DSSCs) are critical power devices since many environmental and energy issues are needed to be addressed [9].

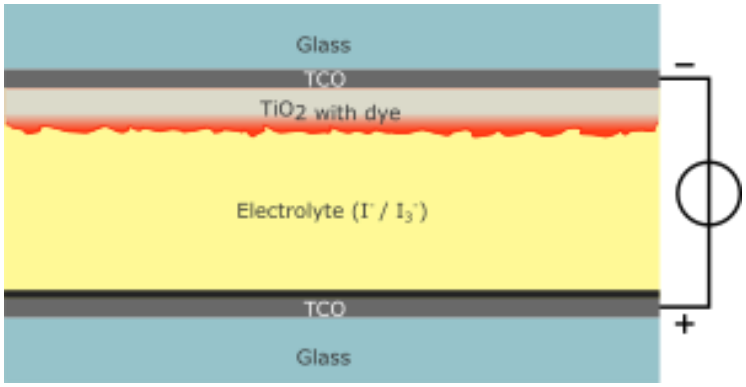

Figure 2.1: Basic structure layer of DSSC

2.2.1 Working principle of DSSC

DSSCs are distinct from traditional semiconductor devices in that they distinguish the light absorption feature from the transport of the charge carrier. The Dye sensitizer absorbs the sunlight incident and uses light energy to induce vector electron transfer [10]. In DSSCs, the dye molecules absorb and get excited by the incident photons on the mesoporous TiO2 layer surface. These excited dye molecules inject an electron into the mesoporous photoanode network's conduction band and oxidize the dye molecules that lose an electron. To enter the counter electrode, these injected electrons migrate to the external load via the TiO2 sheet. The electrons are being transport to the electrolyte, where an electron from I- ion is obtained by the oxidized dye to replace the missing electron. The iodide molecules are oxidized into triiodide I-3 ions at the same time. Finally, at CE (cathode), I-ion regeneration occurs, and electron migration via the external load completes the circuit [11].

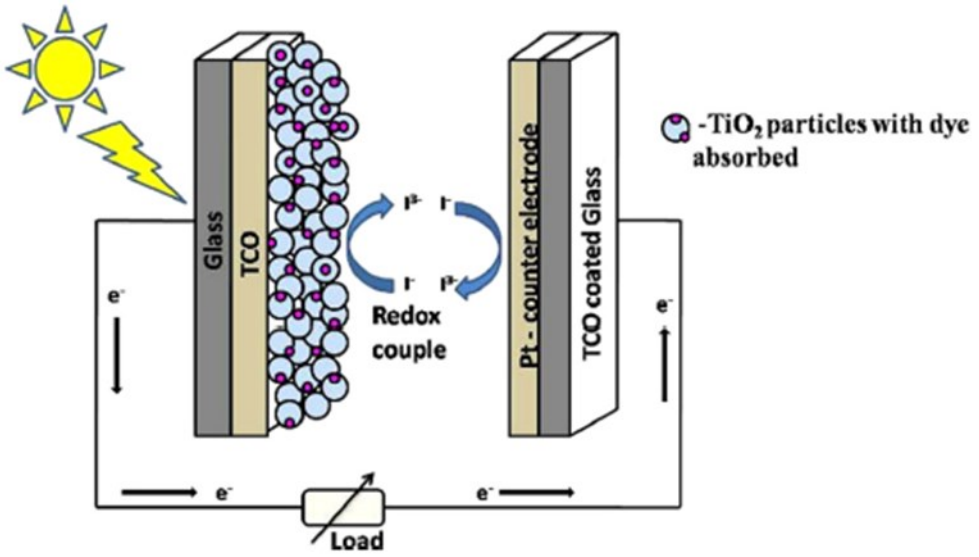

Figure 2.2: Schematic representation of DSSC

2.2.2 Components of DSSC

DSSC can be regarded as a multi-component system by understanding its operating principles and enhance the cell's performance. The components of DSSC were thoroughly studied, both for individually and interaction with other components [12]. When sandwiched with a pair of glass contacts, a working electrode, dye sensitizer, electrolyte, and counter electrode are composed of a DSSC. DSSC is a work electrode assembly sodden with a sensitizer or dye and closed to prevent electrolyte flow to the counter electrode with a thin layer of electrolyte soaked with a hot melt tape [13].

2.2.2.1 Glass contact

Usually, DSSCs are made from two layer of transparent conductive materials that assist a semiconductor and catalyst removal substratum, often serving as current collectors. As a transparent electrode, most solar cells use TCO films. In addition to conductivity and clarity, the critical considerations in choosing the TCO for this

application are electronic unity with adjacent cell layers, processing specifications, and stability under environmental conditions [14]. The two-essential attribute of the substrate used in the dye-sensitized solar cell are: first, the substrate needs more than 80 percent transparency to allow maximum sunlight to pass to the cell's effective area. Secondly, the conductivity of the DSSCs should be huge for efficient transfer of charges and lower energy loss [14]. Transparent conducting oxide (TCO) glasses, such as a fluorine-doped tin oxide (SnO2: F) (FTO), tin-doped indium oxide (In2O3: Sn) (ITO), and aluminum-doped zinc oxide (ZnO: Al) (AZO) glasses, have historically been used as a substrate for DSSCs. The higher cost, brittleness, harshness, and form constraints diminish their practical applications, despite their excellent stability against oxygen and water. Furthermore, it is not possible to use the roll-to-roll development process for this device. Flexible substrates with lightweight and fast transport characteristics have, therefore, become an option [15]. In DSSCs, fluorine-doped tin oxides (FTO, SnO2: F) and indium-doped tin oxides (ITO, In2O3: Sn) are commonly used a conductive substrate. These substrates subsist of lime soda glass glaze with tin oxide layers doped with indium and tin oxide doped with fluorine [14]. FTO is used the most for DSSC applications due to its favorable electricity element and optical clarity. Much research has suggested FTO substrate is remarkable to the indium tin oxide (ITO) substrate as a photoelectrode in DSSCC because of its stability at exalted temperatures. Usually, photoanode preparation requires the deposition and sintering of TiO2 paste on TCO substrates at high temperatures (~450 °C) to rise electrical communication. The sheet resistance of ITO glass will, however, increase enormously when expose to heat treatment at around 300 ° C, leading to lower output [16].

2.2.2.2 Working Electrode

In DSSC, the working electrode is often recognized as a photoanode. Usually, the photo-anode consists of semiconducting broad bandgap metal oxide, normally FTO glass, deposited on the TCO substrate's surface. In order to support the sensitizer load and transport photo-excited electrons from the sensitizer to the external circuit, the photoanode performs dual functions. Therefore, to ensure elevated dye loading, a wide surface area is needed. Furthermore, a rapid charge transport rate is required to provide high electron collection efficiency. The distinguishing characteristics of an ideal photoanode are these two properties [17]. As a semiconductor substrate, mesoporous oxides, including TiO2, ZnO, SnO2, and Nb2O5, are the most used materials. The enormous energy bandgap of these oxides is 3-3.2 eV [13].

Among these, even under extreme operating conditions in photo-electrochemical systems, TiO2 is a robust photoelectrode. However, DSSCs based on nanocrystalline TiO2 have greater efficiency compared to ZnO and SnO2 based DSSCs. TiO2 is affordable, abundant and non-toxic [18]. With the introduction of the first TiO2-based DSSCs by Priorto Grätzel in 1991, Gerischer and Tributsch prospective ZnO as an efficient photoanode option. In TiO2-based DSSCs with big bandgap energy like TiO2 (Eg ≈ 3.37eV) and higher electron mobility compared to TiO2, ZnO can resolve higher electron recombination. Though ZnO efficiencies are still far below that of TiO2 (less than 8%), a few studies have been highlighted by researchers in this field to improve the output of ZnO-based DSSCC power conversion efficiency [19].

With the production of ZnO composite materials and nanostructures in research and technology, due to their low-cost methods of planning, friendliness to the

environment and good results, ZnO has emerged as one of the favorable choices for DSSCs. ZnO composite nanostructures are commonly graded into (a) one-dimensional (1D) nanostructure, (b) two-dimensional (2D) nanostructure, (c) three-dimensional (3D) nanostructure, and (d) hybrid nanostructure. The different characteristics of the TiO2/ZnO composite photoanode nanomaterial nanostructure are shown in *Table 2.3* [20].

Table 2.3: Nature of DSSCs with various nanomaterial ZnO structures [19]

Nanostructure/ Nanocomposite	Materials	V_{oc} (V)	J_{sc} (mA/cm^2)	FF (%)	η (%)
Nanorods	Doped with TiO2 with ZnO nanorods of various sizes	0.76	11.4	0.50	5.8
Nanotubes	-Coaxial TiO2/ZnO nanotube arrays	0.65	7.28	0.60	2.8
	-ZnO/TiO2 nanotube arrays	0.895	5.96	0.704	3.75
	-ZnO-decorated TiO2 nanotubes	0.72	6.77	65.11	3.17
	- TiO2 nanoparticles-coated ZnO nanotube arrays	0.94	6.97	0.60	3.94
Nanowires	- Coated with a thin shell of TiO2 anatase, ZnO nanowire arrays	0.78-0.82	4.0-4.5	0.58-0.6	2.25
	- Arrays of TiO2-coated ZnO nanowires	0.788	12.26.2020	0.587	5.65
Nanofibers	- Nanofibers ZnO core-sheath films	0.75	11.3	0.61	5.17
Nanocomposite	-TiO2 coated ZnO	0.770	8.78	0.724	4.89
	-ZnO coated TiO2 nanoparticles	0.72	0.49	0.69	1.21
	-ZnO coated TiO2	0.75	13.46	0.654	6.62
Nanodonuts	TiO2/ZnO nanodonuts	0.78	16.70	0.69	9.00
Nano flower	-ZnO nanoflowers/TiO2 nanocomposite	0.82	6.14	0.56	2.82
	- TiO2 amorphous/crystalline over the nanoflowers/nanorods of ZnO	0.76	6.303	0.60	3.1
3D hierarchical heterostructure	Deposited 1D ZnO nanorods on 2D TiO2 nanosheets	0.8	3.24	0.17	0.51

Promising elements for DSSC are one-dimensional (1D) nanostructures due to several efficiencies and processing advantages. Due to smooth electron directional mobility, such nanostructures can improve the properties of electron transport. Therefore, it accelerates the transport of electrons and decreases the risk of

recombination. Furthermore, its geometry provides a wide surface area that improves the efficiency of DSSCs in turn. The larger size also leads the effect of light scattering that improves the light adsorption of the dye. They were produced by different methods, TiO2 and ZnO nanotubes, nanorods, nanowires, etc. techniques [21].

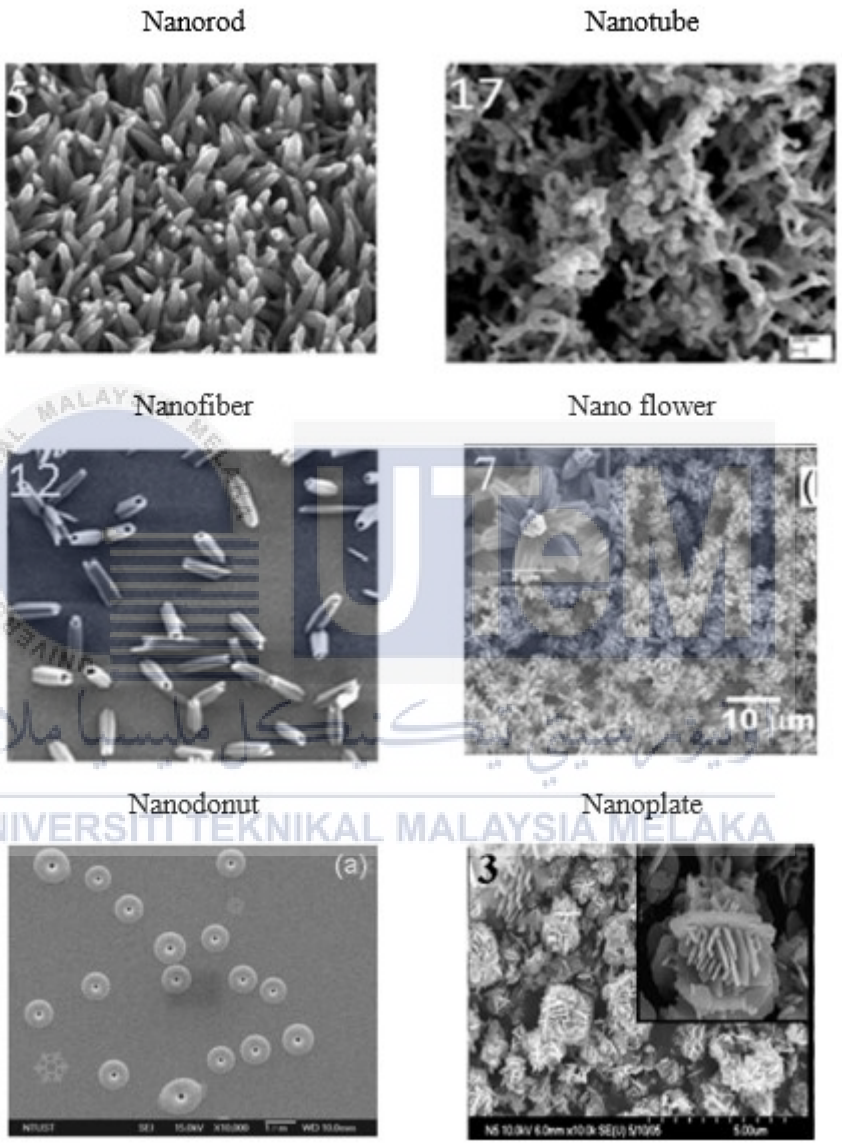

Figure 2.3: Examples of nanostructure morphology with respective SEM image [21]

Several analysts have recently documented nanostructure of two-dimensional (2D) for DSSCs, such as branched nanowires, nanosheets, nanofilms, etc. With

distinct Shape-dependent features that differ from the properties of bulk, the 2D nanostructures have several low dimensional features. They are then used as the primary components of nanodevices. However, the TiO2 and ZnO's 2D nanostructure is not common because of its low photoconversion efficiency [21]. The odd disposal of particles of TiO2 and the resulting structural film anarchy causes an increase in the dispersion of free electrons injected with dye and thus a decrease in electron mobility [15].

Because of their high absorption of dye, large pore volume, excellent dispersion of light and vital optical clarity, porous photoanodes exhibit superior photovoltaic properties during the processing of DSSCs. In three-dimensional (3D) nanostructured materials, basic properties are shown. Through the electrospray process, the investigator synthesized novel sponges such as TiO2/ZnO nanodonuts. The findings indicate a large volume of pore, higher absorption of dye, greater light dispersion, more efficient transport of electrons, and electron penetration properties. 9 percent efficiency of energy transfer is also reached, 44.4 percent higher than P25 particle dependent DSSCs. It is also relatively superior to other morphologies of TiO2/ZnO [21].

Other than TiO2 or ZnO nanostructures, several hybrid structures have been researched by combining different nanostructures. Using the [Co(bpy)3]2+/3+ redox couple (a redox mediator) and porphyrin dye (SM315, green dye) over TiO2 film, DSSCs were recently manufactured with 13 percent PCE at full sun illumination. In visible and near-infrared conditions, that leads to improved light harvesting. Synthesized TiO2/ZnO hybrid heterostructure arrays (TiO2 nanowire/ZnO nanorod or TiO2 nanowire/ZnO nanosheet) have proven to be a high rated solar cells, excellent

nanomaterials. It results in larger surface area, better electricity, which helps to transfer electrons efficiently and diffuse the electrolyte in DSSC, power conversion efficiency of 5.75 percent resulted in (PCE). By contrasting the efficiency of various nanostructures, of TiO2/ZnO, it is noted that due to Superior performance can be seen on DSSCs using a one-dimensional structure with faster electron transfer, slower charge recombination, and greater capability (nanotubes, nanorods, and nanowires). A better DSSCs contain mesoporous TiO2 nanostructure [21].

2.2.2.3 Dye sensitizer

Another essential elements of a DSSC are sensitizers. Sensitizers' primary function is to absorb solar photons and inject the photo-excited electrons into the n-type semiconductor conduction band [12]. The dye is chemically attached to the surface of metal oxide (the semiconductor). To be regarded as an effective photosensitizer, the selected dye must meet several criteria [18]. In recent decades, a wide range of photosensitizers have been studied for DSSC applications: they are possibly the most researched part of a DSSC system. They have been well-reviewed in several articles [12]. A promising DSSC photosensitizer must have a few requirements, such as (1) high absorption coefficient; (2) bigger visible spectrum to absorb sunlight at all wavelengths; (3) the dye's energy level of LUMO must be greater compare to photoelectrode's conductive band energy level; (4) high chemical absorption; (5) optimal viscosity; (6) fast dye generation; and (7) high molar extinction coefficient [20]. Examples of dyes widely used for DSSC are ruthenium-based photosensitizers, metal-free organic sensitizers, quantum dot sensitizers, perovskite-based sensitizers, and natural colours.

Ru (II) polypyridyl dyes show excellent performance as the most common sensitizer for DSSCs due to their large light absorption range from ultraviolet to near-infrared light, suitable energy levels for TiO2 photoanodes and I-/I3- electrolytes, and high molecular stability. The efficiency of Ru(II) dye-based DSSCs had already hit 10.0% by the mid-1990s. in addition to subsequent efficiencies of 11.2% in 2005 and 11.7% in 2010, respectively [17]. Photosensitizers based on Ru carrying hydrophobic groups were investigated in the ancillary ligands [12]. For several reasons, Ru(II) metal is a better study choice: (1) it's octahedral geometric structure tolerates controlled extension of specific ligands; (2) it is possible to tun the photophysical, photochemical, and electrochemical properties of Ru(II) complexes; (3) the oxidation states are stable and available from I to IV; and (4) the solubility of many solvents is strong. [7]. Cis-bis (isothiocyanate)bis-(4,40-dicarboxylic acid-2,20-bipyridine) Ru (II), stand for N3 or red dye, is the first popular Ru-based complex photosensitizer. Afterwards, the same group synthesized the other two effective dyes. One is the black dye with the prescription of tris(isothiocyanate)-2,20,200-terpyridyl-4,40,400-tricarbolylate Ru(II)complex, or denoted as N749 dye, and the other is imply as N719 dye with the formula of di(tetrabutylammonium)cis-bis(isothiocyanate)bis-(4-carboxylic acid-40-carboxylate-220-bipyridine)Ru(2) (II) [15].

The third primary class of photosensitizers for DSSC are metal-free organic dyes. The chemical structure is more easily tunable concerning ruthenium-based sensitizers by leveraging the conventional synthetic strategies used in dye chemistry. The modulation of the chemical properties results in significant optical properties variability to obtain sensitizers with broad spectral absorption [12]. The key advantage of organic dyes is the simplicity of structural modifications that can enhance the efficiency of DSSC. In addition, organic sensitizers show significantly higher

coefficients of extinction than metal-based complexes such as complex Ru sensitizers. The electron acceptor serves as the dock group which binds the dye to the surface of the semiconductor. Facilitating the electron injection into the conduction band of the photoanode and simultaneously timing [12]. Metal-free organic dye 36 containing thienyl ethynyl as a spacer has 4.49 percent efficiency reported for DSSCs. By indicating that as the thiophene unit and length of the conjugated spacer increase, the oxidation, reduction potential and consequently band gap of the molecule diminish compared to other dyes [22].

As a substitute for dye molecules, certain inorganic quantum dots (QDs) have been adopted or combined to form photosensitizers with dye molecules. Besides, co-sensitization would be requite for the limited absorption range of the dye molecule and recognize the relationship between the QDs and dye molecules, undoubtedly improving its overall capacity to absorb light [23]. The only distinction between sensitizing materials (QDSSC) is between the DSSC and the quantum dot sensitized solar cell. Inorganic nanoparticles of QDs in the QDSSC are substituted for the dye. Due to its interesting characteristics, such as moving from excited peak to higher energy, blue change in the saturation band edge, and below picosecond optical transition speeds, the use of QDs as sensitizers. Due to its bulk content bandgap above 1.3 eV, this due to increment photon absorption by CdX. CdS, CdSe, and CdTe, have a band difference of 2.25, 1.73, and 1.49 eV, respectively [7].

Due to their excellent light-harvesting characteristics, halide perovskite sensitizers have recently attracted considerable attention. The first perovskite-sensitized solar cell was recorded in 2009, CH3NH3PbX3 exhibit the PCE of 3.81 percent, which later raised to 6.5 percent during 2011. A significantly improved PCE

of 12.3 percent for solar cells based on perovskite CH3NH3PbX3 was published in 2013 [17]. The ratios between CH3NH3I and PbX2 differed according to the perovskite target to synthesize the perovskite-containing mixed halides. The most popular one-step approach to date is CH3NH3PbI3-xClx, with 20 percent cell PCE [7].

Natural and synthetic dye sensitizers can be differentiated by various parameters, such as cell cost, environmental conditions, the problem of durability, DSSC performance, maximum absorption, accessibility of resources, and production techniques [24]. The dyes are derived from colorful flowers, leaves, fruits, etc., that naturally occur. The colors are due to the presence of various pigments that have verify to be strong photosensitizers. Natural photosensitizers (natural dye) are generally known as carotenoids, betalates, flavonoids, or chlorophylls [18]. The predominant photosynthetic pigments are chlorophylls. Their primary purpose is to absorb and use light for the preparation of starch in the visible region. The capacity to absorb visible light allows to be used as DSSC dyes. Among other chlorophylls, Chl a and Chl b are considered useful dyes for the DSSC application. Even though natural dyes transform on the offsets of other solar generation cells, because of it easier dye aggregation that impacts film absorption, the reported efficiency is inferior. This leads to steric molecular impedance that block its moving on the surface and degrades the color balance over time [20].

Table 2.4: Type of sensitizer for DSSC [7]

DSSC	Sensitizer	Efficiency (%)
DSSC with Ru-complex dyes	cis-X2Bis(2,2′-bipyridyl4,4′-dicarboxylate) ruthenium (II) complexes (X=C1, Br, I, CN)	10
	Ru 2,2′ bipyridine-4,4′ dicarboxylic acid (μ-(CN) Ru (CN) 2,2′ bipyridine)2	7.1
	Di-tetra butyl ammonium cis-bis (isothiocyanate) bis (2,2′-bipyridyl-4,4′-dicarboxylate) ruthenium (II)	11.2
	Dichloro(p-cymene)- ruthenium (II) dimer ([Ru(p-cymene) Cl2]2	7.5
DSSC with metal-free organic dyes	YD2-o-C8	12.5
	4-(bis-(4-bromo-phenyl)-amino)-benzaldehyde	5.35
	As the electron donor, triphenylamine moiety, cyanoacrylic acid as the acceptor of electrons, and novel tetrathienoacene as the π-bridge	10.1
	Phenyl dihexyloxysubstituted TPA (DHO-TPA) Y123	10.3
	Zinc porphyrin dye containing meso-position acrylic acid	5.1
DSSC with quantum-dot dyes	CdS quantum dots	4.22
	CdSe0.45Te0.55 alloyed quantum dots	6.36
	Cadmium nitrate-mixed manganese acetate/CdS/CdSe quantum dots	5.42
DSSC with perovskite-based sensitizers	(CH3NH3) PbI3 + screen printing method	3.8
	(CH3NH3) PbI3 + films	6.54
	(CH3NH3) PbI3 + spin coating method	9.7
DSSC with natural dyes	Mangosteen pericarp	1.17
	Hibiscus surattensis	1.14
	Raspberries	1.50
	Ipomea	0.28

2.2.2.4 Electrolyte

One factor that plays a vital role in DSSCs is an electrolyte in a DSSC because the electrodes' charge transport occurs through it [25]. Generally, electrolytes, such as liquid, quasi-solid state, and solid-state electrolytes, are categorized into many groups. There are five main components of an electrolyte like as I-/I-3, Br-/Br-2, SCN-/ SCN2, and Co (II)/Co (III), i.e., redox pair, solvent, additives, ionic liquids, and cations. There are a few element that an electrolyte should have, i.e. (1) redox pairs are able to effectively generate the oxidized dye, (2) better chemical, thermal and electrochemical stability should be present, (3) need to be gentle with DSSC components, (4) allowing fast dissipation of charging carriers, increase conductivity and build active contact between working components [13]. Generally, electrolytes, such as liquid, quasi-solid state, and solid-state electrolytes, are categorized into many groups.

Due to volatilization issues akin to the operation of DSSC, liquid electrolytes are treated as an important aspect affecting the life and the handling of liquid electrolytes during manufacture is complicated [25]. The iodide-triiodide (I3-/I-) electrolyte can be known as a universal redox transporter due to its good kinetic effects, for example rapid oxidation of I- at the photoanode/electrolyte interface for good color growth and sluggish decrease of I3- at the electrolyte/counter electrode alliance for high carrier collection, great intrusion, more stable, etc. Nowadays, the PCE of I3-/I- electrolyte-based DSSCs has reach 11% efficiency [17].

In liquid electrolytes, the practical application of DSSCs is greatly hampered by stop problems and long-term durability. Therefore, efforts have been geared towards alternatives, i.e., quasi-solid-state electrolytes and solid-state electrolytes, to liquid electrolytes. Ionic liquids containing redox pairs (e.g. 1-propargyl-3-

methylimidazolium iodide, bis(imidazolium) iodides and 1-ethyl-1-methylpyrrolidinium) and polymer gel (e.g. poly(ethylene oxide), poly(vinylidene fluoride) and polyvinyl acetate) are widely used as quasi-solid-state electrolytes to resolve liquid electrolyte agitation and exposure concerns [17].

To prevent the disadvantages of ionic liquid (IL) electrolytes, solid-state electrolytes are built [13]. Solid-state electrolytes, include different hole-transporting materials, have been broadly studied as hole acceptors to change liquid electrolytes (HTMs). In solid-state DSSCs, some inorganic p-type materials (e.g., CuI/CuSCN and CsSnI3) and organic polymers (e.g., poly (3,4-ethylene dioxythiophene) (PEDOT), 2,20,7,70-tetrakis (N, N-di-4-methoxyphenylamino)-9,90-spirobifluorene (spiro-MeOTAD), and poly(3-hexylthiophene) (P3HT)) were successfully used (SS-DSSCs). Fast crystallization speeds, however, resulting in a lesser filling of photoanode films, and so SS-DSSCs have a low efficiency of 3.8 percent. CsSnI3, which has high hole mobility, less weight, sufficient raw materials, and inexpensive manufacturing show a encouraging p-type semiconductor HTM. Such electrolyte-based devices allowed up to 10.2 percent PCE in 2012, for SSDSSC [17].

2.2.2.5 Counter electrode

The counter electrode has the critical purpose of collecting electrons from external circuit in DSSCs and catalyze the redox reduction at the electrolyte. The primary requirements of CE materials are high charge transport conductivity, strong electrocatalytic behavior for the reduction of redox couples, and excellent stability [17]. In DSSCs, CE was often used platinum (Pt) or carbon (C). Working electrodes are closed together with counter electrodes and a syringe is then filled with an electrolyte. The counter electrode activate the reduction of I-/I-3 liquid electrolytes

and gathers gaps from the transport materials of the void [13]. Noble metals, such as Pt, Au, and Ag, are the common because of their high electrocatalytic activity (e.g., Pt) for reducing redox couples in liquid electrolytes or effective hole transfer in solid-state electrolytes (e.g., Au and Ag) [17]. As it shows greater efficiencies, Pt is needed as the counter electrode resulting the need for the substitution of Pt was needed considering its expensive price and lower affluence. Therefore, several option to replace Pt have been produced, such as carbon, carbonyl sulfide (CoS), Au/GNP, CE alloys such as FeSe $CoNi_{0.25}$ [13]. Due to their superior characteristics, such as good electricity element, inexpensive, excellent stability and high catalytic activity for I^{-3} reduction, polymers such as poly(3,4-ethylene dioxythiophene) (PEDOT), PEDOTdopedwithpoly(4-styrene sulfonate) (PEDOT: PSS), polypyrene(PPy), polyaniline (PANI), and poly(3,4 propylenedioxythiophene)(ProDOT) have been used as the CE catalyst for DSSCs [15]. Several carbon aceous materials have been tried as alternative counter electrode materials, such as carbon black, activated carbon, graphite, carbon nano tubes, and graphene. Compared to Pt, carbon materials used as counter electrodes show weaker catalytic action. It can be offset by an increase in the catalytic layer's active surface area using a porous structure. To have comparable efficiencies of Pt counter electrodes, these carbon counter electrodes going to be short a few mm compactness greater than Pt counter electrodes [11]. However, the key downside of carbon-based CE is the need for a bigger doses to achieve the desire catalytic activity and the weak relation among carbon film and its substrate [15]. Below are the photovoltaic specification for the DSSCs that use composite CE [17].

Table 2.5: DSSCs photovoltaic output using composite counter electrode [17]

Counter Electrode	PCE (%)	vs. Pt (%)
Graphene-TaON	7.65	7.91
Graphene-NiS2	8.55	8.15
Graphene-PPy	5.27	6.02
Graphene-NiO	7.42	8.18
CNTs-graphene	8.23	7.61
CNTs-NiS	7.90	6.36
CNTs-WS2	6.41	6.56
CNTs-PEDOT: PSS	8.3	7.50
CNTs-TiN	5.41	5.68
PEDOT: PSS-CuInS2	6.50	6.51
PEDOT: PSS-TiN	6.67	6.57
PEDOT: PSS-CoS	5.40	6.10

2.2.3 Parameter of DSSC

The completion of a DSSC can be analyzed using incident photon to current conversion efficiency (IPCE, percent), short circuit current (Jsc, cm-2), open circuit voltage (Voc, V), maximum power output [Pmax], total efficiency [Pa, percent], and fill factor [FF] [13]. Without current flow, the VOC is measured and is the maximum voltage that can be given to an external circuit by the DSSC.

$$V_{oc} = V_T \ln(1 + \frac{J_{sc}}{J_o})$$

Jsc is the overall output current of a DSSC and is part at zero voltage around the cell under illumination. Abs(λ) is the sensitizer absorption, e is the electron charge, and φ(λ) is a normal AM 1.5 irradiance spectrum as a function of the wavelength (λ) and then charge collection is IQE(λ).

$$J_{sc} = \int (1 - 10^{-Abs})) \times IQE(\lambda) \times e \times \phi(\lambda) d\lambda$$

$$I_{sc} = J_{sc} \times A$$

The maximum power output (Pmax) is the peak current and voltage product. Pmax can be calculated with the following equation:

$$P_{max} = I_{mp} \times V_{mp}$$

I_{mp} and V_{mp} are the maximum power of current and voltage values. The ratio of several electrons movement through the external circuit to the number of photons occurring on the surface of the cell at any wavelength is called external quantum efficiency (IPCE). It is given as follows:

$$IPCE\%(\lambda) = 1240 \times \frac{I_{sc}}{P_{in}}$$

The total efficiency (percent) is also the percentage of solar energy that is converted into electrical energy, where the JSC value decreases and the VOC, FF, and molar dye coefficients increase in importance, respectively.

$$\eta(\%) = \frac{P_{max}}{P_{in}} = \frac{I_{mp} \times V_{mp}}{P_{in}} = \frac{I_{sc} \times V_{oc} \times FF}{P_{in}} \times 100$$

Apart from Voc, Isc, and η, fill factor (FF) is the parameter determining a solar cell's performance. The value of FF can be gain from equation:

$$FF = \frac{Area\ A}{Area\ B} = \frac{V_{mp} \times I_{mp}}{I_{sc} \times V_{oc}}$$

2.3 Chitosan

Chitin and Chitosan are polysaccharides that, with relatively good processability, have interesting inherent properties. Besides, these polymers' fascinating surface for diverse and simple applications, flexibility can be tailor-made. Many researchers have created sustainable, eco-friendly, reasonably easy-to-use, functional goods that possibly succeed conventional, non-ecological products in biomedical, environmental and energy applications with these attractive features [26].

2.3.1 Introduction of Chitosan

Chitosan is a natural polysaccharide with a definite structure that is linear. Chitosan molecular chains can interconnect with each other via hydrogen bonds [27]. Chitosan is a polysaccharide consisting principally of 2-deoxy-2-amino-Dglucopyranose units connected to β-(1,4). Chitosan can be considered the most environmentally friendly binder, and aqueous slurries based on its excellent viscosity [28]. Chitosan is predominantly d-glucosamine, which is distinguished by chitin's degree of acetylation (DA). The second most adequate natural biopolymer is chitin, as it is the precursor of chitosan. It is extracted from exoskeletons such as crustaceans, insects, molluscs, certain funguses, etc. Chitin has a degree of deacetylation and was referred to as N-acetyl-d-glucosamine [26]. The relationship between chitin and protein in a polysaccharide-protein complex is very personal, and a small portion of protein is involved as well. In some instances, to eliminate residual pigments, an additional step of decolourization is added. By using chemical or enzyme, both deproteinization and demineralization may be accomplished. Chitin can be change to Chitosan by enzymatic preparations or the chemical process. Chemical methods are widely used for marketing purposes of chitosan preparation due to its inexpensive and propriety for mass manufacture. [29].

2.3.2 Role of Chitosan in DSSC

Gratzel's cell or dye-sensitized solar cells (DSSC), published in 1991, has attracted numerous academic researcher due to its low-cost production with significant efficiencies proportionate to conventional solar cells. Chitosan is a cheap material with abundant nature that is easy to produce. Not to forget to note that it is environmentally safe to research as a polymer host for ion conduction [30]. Chitosan was also used to connect electrodes. Most of the researchers used Chitosan as the electrolyte-based parameter.

Table 2.6: Example of chitosan practice in DSSCs

Used of Chitosan	J_{sc} ($mAcm^{-2}$)	V_{oc} (V)	Efficiency, η (%)	Fill factor, FF
Chitosan polymer electrolyte with ZnO nanostructures DSSC [31]	7.74 (5 wt.% ZnO: Li with N719 dye)	0.64 (5 wt.% ZnO: Li with N719 dye)	5.58 (5 wt.% ZnO: Li with N719 dye)	42.8 (5 wt.% ZnO: Li with N719 dye)
Chitosan-based gel polymer electrolyte with TiO2 [25]	20.33 (PhCh-based gel polymer electrolyte)	0.37 (PhCh-based gel polymer electrolyte)	3.57 (PhCh-based gel polymer electrolyte)	65 (PhCh-based gel polymer electrolyte)
Chitosan NH41 biopolymer electrolyte [30]	4.55 (50wt% [chitosan-NH4I] with N3 dye)	0.64 (50wt% [chitosan-NH4I] with N3 dye)	1.20 (50wt% [chitosan-NH4I] with N3 dye)	0.40 (50wt% [chitosan-NH4I] with N3 dye)
Chitosan based polymer electrolyte for natural DSSC with TiO2 [8]	6.4 (solid electrolyte)	0.53 (solid electrolyte)	1.80 (solid electrolyte)	53 (solid electrolyte)
Chitosan binder-based TiO2 electrode [28]	10.15 (2 wt.% of chitosan)	0.69 (2 wt.% of chitosan)	4.16 (2 wt.% of chitosan)	59.41 (2 wt.% of chitosan)
Hexanoyl chitosan and NaI blends for solid state DSSC with TiO2 [32]	8.62 (30wt% of NaI)	0.58 (30wt% of NaI)	2.98 (30wt% of NaI)	62 (30wt% of NaI)

2.4 Research summary

Table 2.7 below shows some recent research related to synthesis of chitosan binder-based ZnO for dye-sensitized solar cell. DSSC based on zinc oxide got many interests from researchers because the output result from this topic can be a steppingstone to increase the DSSC performance. Most of the researcher are more interested toward the use of chitosan as polymer, dye sensitizer, and electrolyte. In contrast, chitosan binder-based electrode got less attention and having lesser progress through the years.

From previous research, there are many methods to synthesis of chitosan, some of the preparation method is straightforward and does not involve complicated materials and equipment while some are complex. There are also researches on improving the current standard chitosan. In 2020, there is a research on the characteristic of chitosan-ZnO nanocomposites where it focuses on dielectric, mechanical, and piezoelectric effects.

Furthermore, in 2013, efficiency of 4.16% have been achieved with chitosan binder-based titanium dioxide electrode with 2.0 wt.% of chitosan. This indicated that the use of chitosan as electrode binder can be progress to achieve a higher efficiency dye-sensitized solar cell.

Table 2.7: Related past research

Years	References	Approaches	Results
2013	Preparation and Characterization of Chitosan Binder-Based TiO2 Electrode for Dye-Sensitized Solar Cells [28]	For DSSCs, chitosan has been selected as a new electrode binder.	Different amount of chitosan shows different efficiency. 1.5wt%=3.83% 2.0wt%=4.16% 2.5wt%=3.94% 3.0wt%=3.29
2017	Preparation and Charaterization of Chitosan from Shells of Shrimp [33]	Using shrimp shell to synthesis chitosan	As white powder with adequate physio hematic characteristics, chitosan was obtained: ash content below 0.063%; insolvent content of 0.62% or less; deacetylation levels above 90%; and crystallinity index around 40%.
2020	Improved Method for Production of Chitin and Chitosan from shrimp shells [34]	Pretreatment procedures examined prior to the standard Chitin and Chitosan production	The prepared chitin and chitosan show a high purity with very low ash (<0.3%) and residual proteins (<0.5%).
2020	Chitosan-ZnO Nanocomposites Assessed by Dielectric, Mechanical, and Piezoelectric Properties [35]	Structural characterize nanoparticles of chitosan-zinc oxide at a wide variety of levels of nanoparticles.	In NO-NCs films, the piezoelectric coefficient is 15 wt.% higher than most nanocomposites polymer-ZnO.

CHAPTER 3

METHODOLOGY

3.1 Introduction

This chapter clarify the procedure, methods and materials used in the synthesis process of chitosan and zinc oxide quantum dots. There are two main process which are synthesis of chitosan from dried shrimp shells and fabrication of DSSC. Both samples will be tested using XRD, SEM, FTIR and UV-Vis to identify its morphology and characteristics.

3.2 Experimental materials and equipment

The tables below show the list of chemicals used in this study. All the chemicals were used without any further modification.

Table 3.1: List of materials for Chitosan

No.	Materials	Formula
1	Shrimp shell	-
2	Hydrochloric acid	HCl
3	Sodium hydroxide	NaOH
4	Ethanol	CH3CH2OH
5	Distilled water	H2O

Table 3.2: List of devices and equipment's used

No.	Device and equipment
1	Electronic Scale
2	Digital Multimeter
3	Ultrasonic Bath
4	Hotplate Stirrer
5	Spin Coater
6	Oven
7	X-Ray Diffraction (XRD)
8	Scanning Electron Microscope (SEM)
9	Fourier-transform Infrared Spectroscopy (FTIR)
10	Ultraviolet-visible Spectroscopy (UV-Vis)

3.3 Experiment procedure

In this section of the chapter, the procedure and method used for this experiment will be explain through diagram and flowchart.

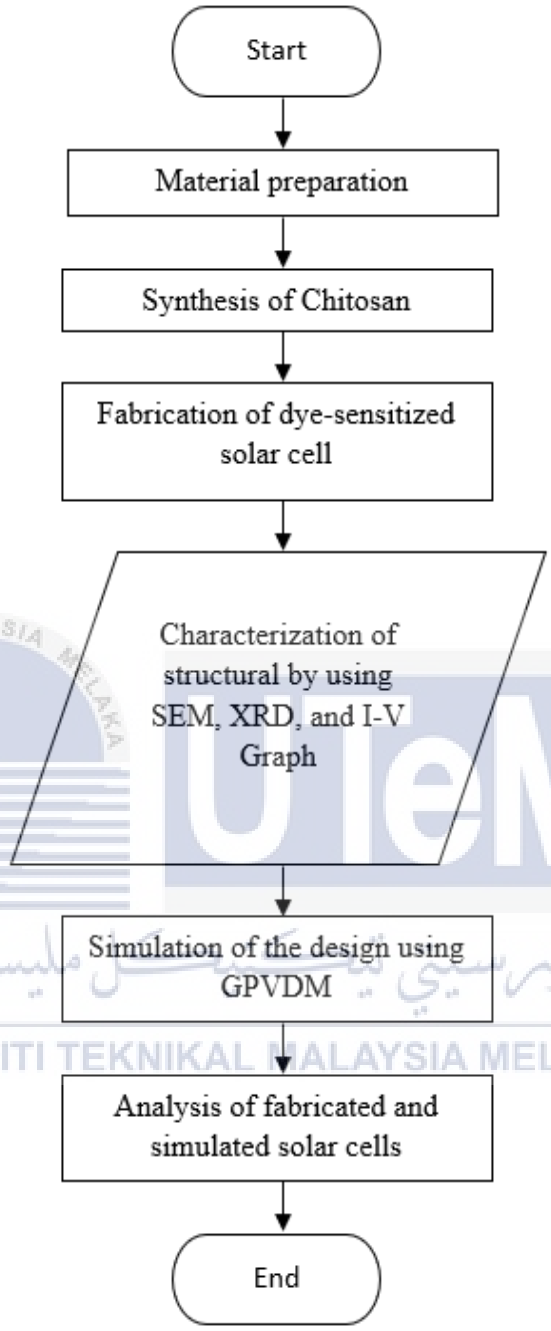

Figure 3.1: Flowchart of the experiment procedure

3.4 Chitosan

Chitosan is a polysaccharide made from chitin, where it is the world's second most prevalent polysaccharide after cellulose. Chitosan is non-toxic, biocompatible, and biodegradable.

3.4.1 Synthesis of chitosan flowchart

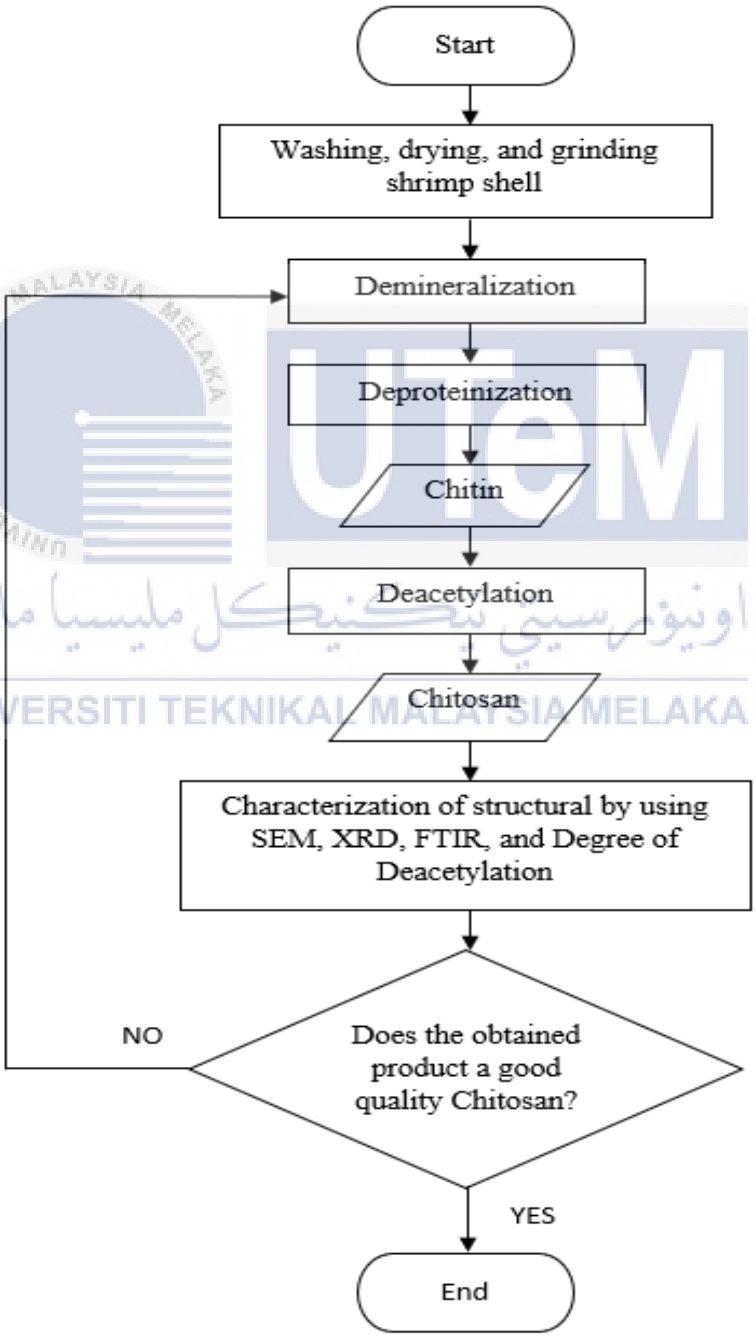

Figure 3.2: Flowchart diagram of chitosan synthesis

3.4.2 Preparation of chitosan

There are four important step for the synthesis of chitosan. The step is in sequence of dried shrimp shell preparation, demineralization, deproteinization, and deacetylation. There are 4 different recipes that have been change from the original recipe by De Queiroz Antonino, R. [33]. *Table 3.3* show the differences between the modified recipe and the original recipe.

Table 3.3: Different methods of obtaining chitosan

Process / Samples	Demineralization	Deproteinization	Deacetylation
De Queiroz Antonino, R. [33]	-Add 1L of 1M HCl to 100g shrimp shells. -Agitated at 250rpm for predetermined times (0.5, 2, or 6hrs) under room temperature. -The shells were filtrated and washed with distilled water until neutral pH. -The shells were immersed in ethanol for 10mins and dried in an oven at 70° C.	-Add 1M of NaOH to the dried demineralize shells at solid/liquid ratio of 1:10(g/mL). -Agitated at 80° C for 3hrs -The solid was filtrated and washed with distilled water until achieved neutral pH. -The shells were immersed in ethanol for 10mins, and the resulting chitin was dried in oven at 70° C.	-Add 12.5M NaOH with solid/liquid ratio of 1:15(g/mL). -The mixture was cooled down and kept frozen at -83° C in an ultra-freezer for 24hrs. -After 24hrs, the temperature was raised to 115° C and agitated at 250rpm for 4 or 6hrs. -The resulting chitosan was filtrated, washed with distilled water until neutral pH and dried in oven at 70° C.
Sample 1	**Demineralization 1** -agitate 10g of DSS with 80ml of HCl for 5hrs with 250rpm at room temperature. -filtered with distilled water until neutral pH. -immersed with ethanol for 20 mins and filtered once. -Drying for 8hrs at 70°C	**Deproteinization 1** -Dilute 8g NaOH with 100ml distilled water (2 M NaOH solution) -agitate the dried sample with the solution for 2hrs at 80°C -let soak for 22hrs at room temperature. -filtered using membrane filter	-Dilute 25g NaOH with distilled water to achieve 50ml solution (12.5 M NaOH solution) -agitate the dried sample with the solution for 2hrs at 80°C with 250rpm. -let soak for 1 day -filter the resulting chitosan until neutral

	Demineralization 2 -weight the dried sample. -agitate 30ml HCl with the sample for 2hrs with 250 rpm at room temperature -filtered until neutral pH and immersed in ethanol for 10 mins and filtered again. -drying for 8hrs at 70°C	apparatus until neutral pH. -immersed in ethanol for 10 mins and filtered once. -Drying for 8hrs at 70°C **Deproteinization 2** -Dilute 2g NaOH with distilled water to achieve 50ml solution (1 M NaOH solution) -agitate the dried sample with the solution for 2hrs at 60°C -let soak for 2-3 days period -filter until neutral pH and immersed in ethanol for 10mins -drying for 8hrs at 70°C	pH and dried for 8hrs at 70°C
Sample 2	-agitate 10g of DSS with 80ml of HCl for 5hrs with 250rpm at room temperature. -filtered with distilled water until neutral pH. -immersed with ethanol for 10 mins and filtered once. -Drying for 10hrs at 70°C	-Dilute 8g NaOH with 100ml distilled water (2 M NaOH solution) -agitate the dried sample with the solution for 2hrs at 80°C -let soak for 24hrs at room temperature. -filtered using membrane filter apparatus until neutral pH. -immersed in ethanol for 10 mins and filtered once. -Drying for 8hrs at 70°C	-Dilute 30g NaOH with distilled water to achieve 60ml solution (12.5 M NaOH solution) -agitate the dried sample with the solution for 2hrs at 115°C with 250rpm. -let soak for 2 days period -filter until neutral pH. -immersed in ethanol for 10mins and filtered once. -drying for 8hrs at 70°C
Sample 3	-agitate 10g of DSS with 80ml of HCl for 5hrs with 250rpm at room temperature. -filtered with distilled water until neutral pH. -immersed with ethanol for 10 mins and filtered once. -Drying for 8hrs at 70°C	-Dilute 8g NaOH with 100ml distilled water (2 M NaOH solution) -agitate the dried sample with the solution for 2hrs at 80°C -let soak for 5 days at room temperature. -filtered using membrane filter apparatus until neutral pH.	-Dilute 25g NaOH with distilled water to achieve 50ml solution (12.5 M NaOH solution) -agitate the dried sample with the solution for 2hrs at 80°C with 250rpm. -let soak for 2 days period -filter until neutral pH.

		-immersed in ethanol for 10 mins and filtered once. -Drying for 8hrs at 70°C	-immersed in ethanol for 10mins and filtered once. -drying for 8hrs at 70°C
Sample 4	-agitate 10g of DSS with 80ml of HCl for 5hrs with 250rpm at room temperature. -filtered with distilled water until neutral pH. -immersed with ethanol for 10 mins and filtered once. -Drying for 8hrs at 70°C	-Dilute 8g NaOH with 100ml distilled water (2 M NaOH solution) -agitate the dried sample with the solution for 2hrs at 80°C -let soak for 7 days at room temperature. -filtered using membrane filter apparatus until neutral pH. -immersed in ethanol for 10 mins and filtered once. -Drying for 8hrs at 70°C	-Dilute 25g NaOH with distilled water to achieve 50ml solution (12.5 M NaOH solution) -agitate the dried sample with the solution for 2hrs at 80°C with 250rpm. -let soak for 5 days period -filter until neutral pH. -immersed in ethanol for 10mins and filtered once. -drying for 8hrs at 70°C

3.4.2.1 Dried shrimp shell

The process starts with washing 3kg of shrimp by taking only the body, tail and the head without any meat and internal organs. Clean with tap water until there no other unwanted fluid of the shrimp. Evaporate the shrimp in oven at 90°C for 8 hrs. Total weight after drying was 70 grams.

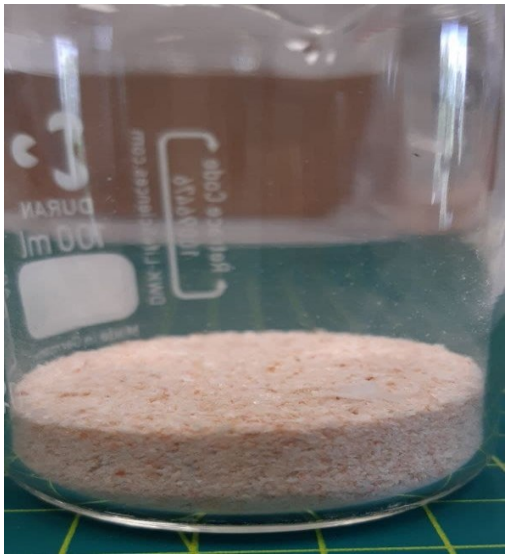

Figure 3.3: Dried shrimp shell

Grind the dried shrimp shells using kitchen blender as fine as it could. After that, keep the dried shrimp shell into cold place to keep the moisture in balance.

3.4.2.2 Demineralization

The process starts by weighting 10g of dried shrimp shells and added 80ml of HCl. Agitated them for 5hrs at 250rpm at room temperature on the magnetic stirrer. After 5hrs, filter the mixture with distilled water using filter paper until pH neutral was achieved. Checked the pH value changes using pH paper. Fully immersed the filtered shrimp shells with ethanol for 10mins. Filtered once with distilled water and put in oven for 8hrs at 70°C.

Figure 3.4: Mixture of dried shrimp shell

Figure 3.5: Demineralized dried shrimp shell

3.4.2.3 Deproteinization

Mix 8g of NaOH flakes with 100ml distilled water to obtain 2M NaOH solution. Added the dry demineralize shrimp shells into 2M NaOH solution and agitated

together for 2hrs at 80°C with 250rpm. After 2hrs, let the mixture soak at room temperature for 5 days. After approximately 5 days of soaking, filter the mixture using membrane filter apparatus until neutral pH achieved with distilled water. Checked the pH value changes using pH paper. Fully immersed the filtered mixture with ethanol for 10mins. Filter the mixture once with distilled water and let dehydrated in oven for 8hrs at 70°C. Chitin was obtained.

Figure 3.6: Chitin

3.4.2.4 Deacetylation

Mix 25g of NaOH flakes with distilled water to achieved 50ml of 12.5M NaOH solution. Mix chitin with the 12.5 M NaOH solution and agitated together for 2hrs at 80°C with 250rpm. Let the mixture for 2 days at room temperature. After 2 days, filter the mixture using membrane filter apparatus until neutral pH achieved. Checked the pH value changes using pH paper. Fully immersed the filtered mixture with ethanol for 10mins. Filtered the mixture once with distilled water and let dehydrated in oven for 8hrs at 70°C. Chitosan was obtained.

Figure 3.7: Chitosan

Degree of deacetylation of chitosan can be calculated using the proposed formula by De Queiroz Antonino, R. [33]. The data need to calculate the formula can be taken from the transmittance spectrum obtain from FTIR analysis.

$$DA(\%) = \left(\frac{A_{1655}}{A_{3450}}\right) \times \left(\frac{100}{1.33}\right) \qquad (Equation\ 1)$$

In this equation, A_{1655} and A_{3450} represent the absorbance of chitosan at 1655 cm^{-1} and 3450 cm^{-1}, respectively.

3.5 Preparation of samples

There are three main samples need to be made which are chitosan layer, ZnO layer, and chitosan-ZnO layer.

3.5.1 Chitosan layer

Dissolved 30mg of chitosan powder in 1ml acetic acid. Added 10ml of distilled water and 90ml ethanol into the dissolved chitosan powder. Stirred the mixture on the

magnetic stirrer for 1hr. Apply 5 drops of chitosan solution for each substrate to ensure its fully coated during the spin coating process. Anneal the coated substrate at 60℃ for 10mins on the hot plate.

3.5.2 ZnO layer

Apply 5 drops of ZnO solution for each substrate during the spin coating process. Anneal the coated substrate at 60°C for 10mins on the hot plate.

3.5.3 Chitosan-ZnO layer

Mix 0.1ml acetic acid with distilled water to produce total volume of 10ml 1% V/V acetic solution. Further, add chitosan (g) into the solution and mix for 1hr at room temperature using magnetic stirrer. After an 1hr, add 0.5g ZnO into the chitosan solution and further stirred until well mix together at room temperature

Table 3.4: Chitosan-ZnO solution mixture

Chitosan (g)	Acetic solution (ml)	ZnO (g)	% wt. of Chitosan-ZnO
0.1	10	0-5	6%
0.2	10	0.5	7%
0.3	10	0.5	8%
0.4	10	0.5	9%
0.5	10	0.5	10%

3.6 Fabrication of dye-sensitized solar cell

There are a few steps for fabrication of dye-sensitized solar cell. It starts by the preparation of ITO glass, followed by preparation of natural dye solution, electrolyte, depositing of photoanode and photocathode, and assembling of the solar cell.

3.6.1 Preparation of ITO glass substrate

Cut an Indium Tin Oxide (ITO) glass with measurement of 1.5cm X 2.0cm. Determine the conductive side of the glass by measuring its sensitivity using digital

meter. The function of measuring resistivity is to ensure that the ITO can conduct electricity, and there is no misplaced side during deposited. Compared to the non-conductive side, the conductive side usually has much less resistance.

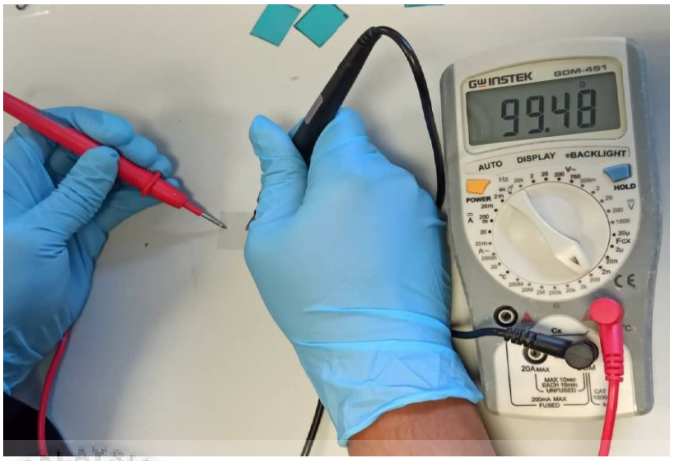

Figure 3.8: Measuring resistivity of ITO glass

Next, clean the ITO glass substrate by dipping into acetone, and then fully soaked the substrate with ethanol. Place the substrate in a beaker facing upward and prevent any overlapping between each substrate. At the temperature of 50°C, put the beaker in the ultrasonic bath for 10mins. After the chemical cleaning process, the substrate then is removed from the beaker by a clean tweezer. Next, put the substrate on the hot plate for drying process with temperature of 50°C.

Figure 3.9: ITO glass soaked in ethanol during sonication

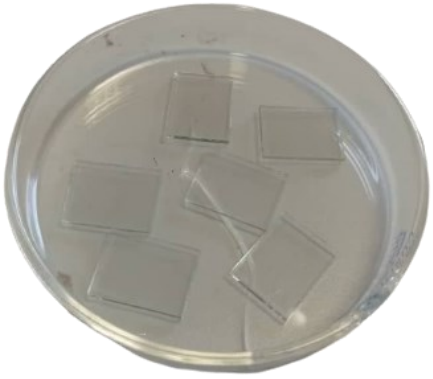

Figure 3.10: Cleaned ITO glass

3.6.2 Preparation of natural dye solution

Prepare a pack of blueberries or any suitable fruit or flower to make a natural dye solution. Clean the berries with tap water for a few times. Put the cleaned berries in a beaker or mortar and crush them using pestle as shown in *Figure 3.11*. After the berries have been mashed nicely, add 6ml of 95% ethanol and 6ml of 15% acetic acid.

Figure 3.11: Crushed blueberries

Figure 3.12: Mixing blueberries with ethanol and acetic acid

Mix well for a few minutes until the solution looking evenly together. Filter the mix solution to separate the solid and liquid using filter paper as shown in *Figure 3.13*.

Figure 3.13: Filter the mix solution

Figure 3.14: Natural dye solution

3.6.3 Preparation of electrolyte

Electrolyte solution needed potassium bromide and deionized water. Weight 5g of potassium bromide. Measure 10ml of deionized water. Add deionized water bit by bit into the potassium bromide while stirring the mixture together. Sonicate the electrolyte mixture for 10 minutes at temperature of 40°C.

Figure 3.15: Mixing potassium bromide with deionized water

Figure 3.16: Sonicate the electrolyte mixture

3.6.4 Depositing and annealing of substrate

There are two substrate in dye-sensitized solar cell which are, photoanode and photocathode. Each substrate will be deposited with different material, where chitosan-ZnO for the photoanode and Graphene Oxide (GO) for the photocathode.

3.6.4.1 Photoanode substrate

Prepare ZnO pasted by mixing 1g of ZnO powder with 10ml of 95% ethanol. After that, put 5 drops of ZnO paste on a cleaned ITO glass. Put the ITO glass in the spin coater machine. Set the machine at the speed of 800rpm for 60 seconds.

Figure 3.17: Spin coating machine

After spin coating, anneal the coated ITO glass on the hot plate for 10 minutes at temperature 60°C.

Figure 3.18: Annealing on the hot plate

Then, let the heated glass for a few minutes and let it fully soak in a beaker of natural dye solution for 30 minutes. After 30 minutes, put the ITO glass on top a piece of tissues to absorb any natural dye solution excess.

Figure 3.19: Soaked in natural dye solution

3.6.4.2 Photocathode substrate

For the counter electrode, firstly weight 3mg of graphene oxide and measure 1.5ml of deionized water to make a graphene oxide solution. Mix material together in a beaker. Sonicate the beaker in the ultrasonic bath for 1 hour at temperature 50°C.

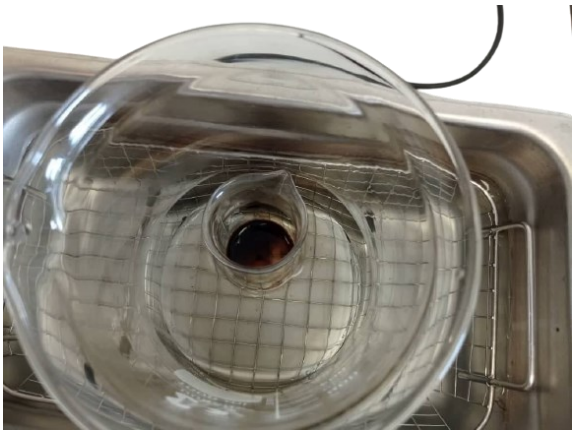

Figure 3.20: Sonicate graphene oxide

After 1 hour, put 5 drops of GO solution on a cleaned ITO glass. Put the ITO glass in the spin coater machine. Set the machine at the speed 800rpm for 60 seconds.

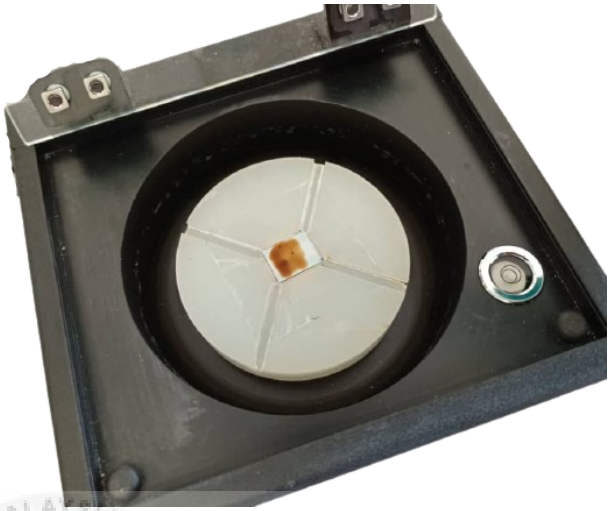

Figure 3.21: Depositing GO solution using spin coating machine

After spin coating, anneal the coated ITO glass on the hot plate for 10mins at temperature 60°C. After 10 minutes, let the ITO glass cooled for a few minutes.

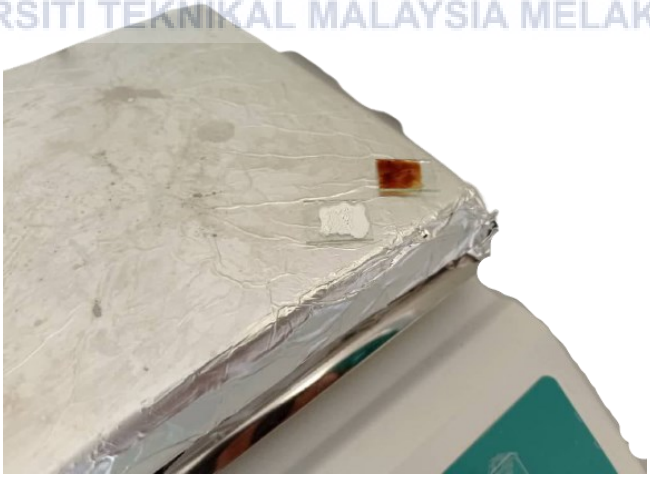

Figure 3.22: Annealing graphene oxide substrate

3.6.5 Final assembling

For the final assembly of the device, sandwiched both photoanode and photocathode substrate together with coated side of the glass facing each other. Clip both part together with a pair of binder clip as shown in *Figure 3.23*. Using a syringe, put electrolyte solution in between the sandwiched glass until it fully covers the connected area. The dye-sensitized solar cell device was ready to be tested.

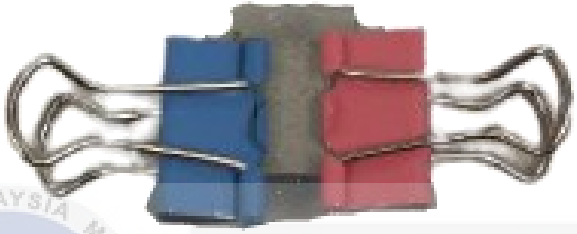

Figure 3.23: Fully assemble dye-sensitized solar cell

3.7 Simulation using GPVDM

3.7.1 Material Parameter

The software requires absorbance data and refractive index of the material to be added to its material libraries. The needed data can be referred from website or any journal which have graphical spectrum where the data can be extracted. The data from the chitosan were extracted from graphical spectrum for absorbance and refractive index [36][37]. There are two electrical where alter during the simulation.

Table 3.5:Electrical parameter of the material

Material	Bang gap (eV)	Electron affinity (eV)
ZnO	3.37[38]	4.51[39]
Chitosan	7.45[40]	-1.1[40]

3.7.2 Layering of Material

There are two type of organic solar cell that been simulated. The first solar cell will consist of only ZnO as the photoanode. The second solar cell will consist of an additional layer of chitosan with different thickness. *Figure 3.24* and *Figure 3.25* show the layering for both organic solar cell.

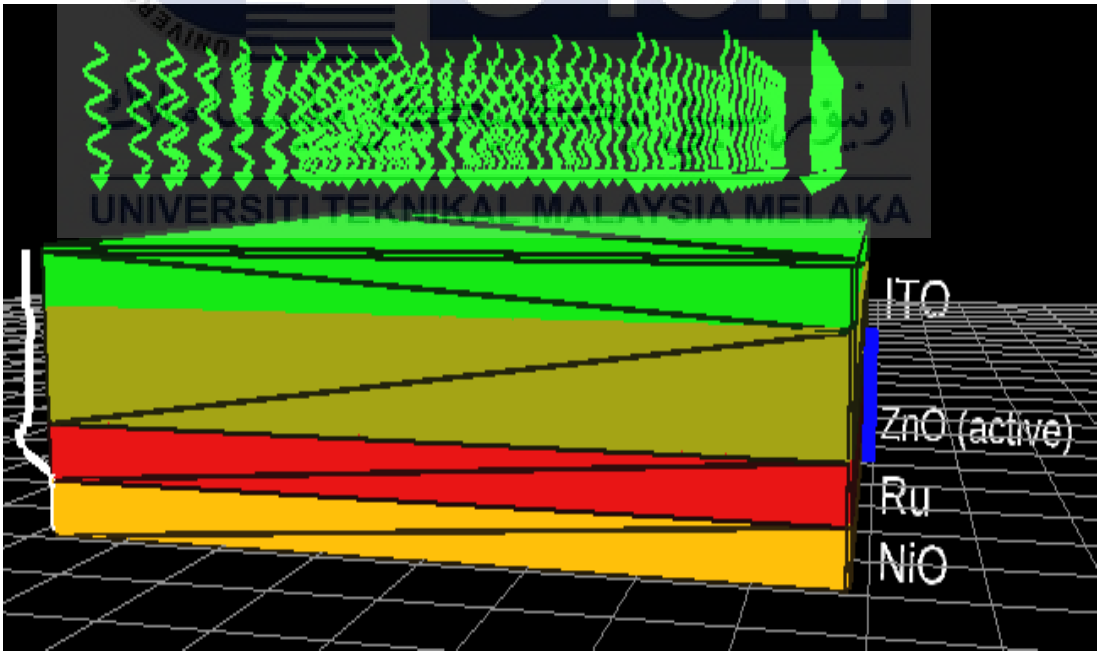

Figure 3.24:Organic solar cell layer with ZnO as photoanode

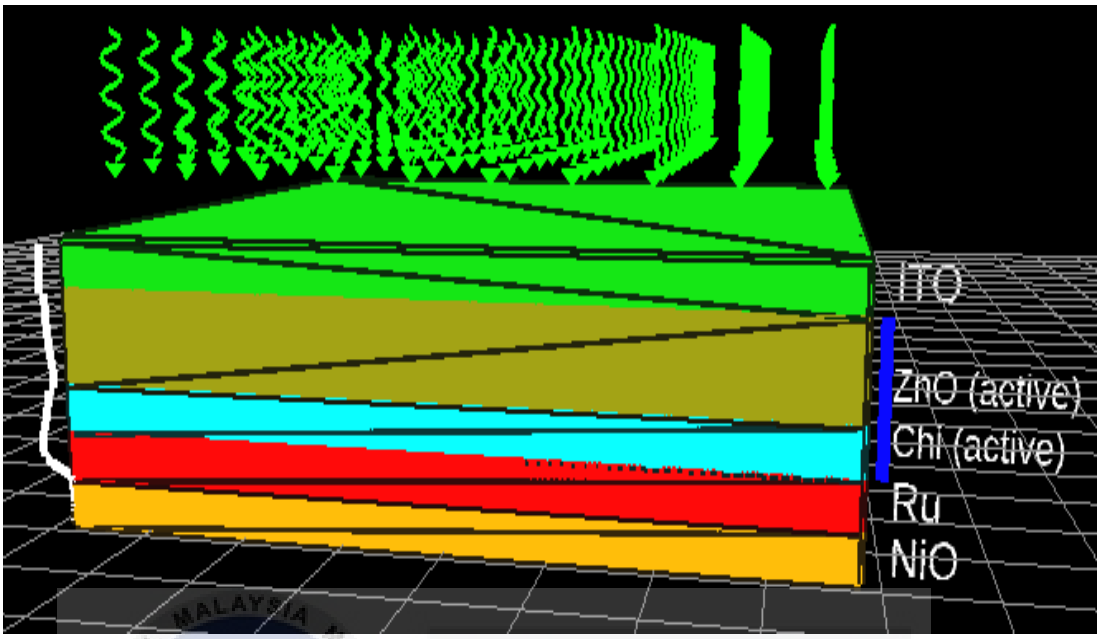

Figure 3.25:Organic solar cell with additional layer of Chitosan

3.8 Safety precaution

Figure 3.26: Laboratory safety equipment

I. Always wear protective clothing including a face mask, safety glasses, chemical gloves and apron while handling the chemical.

II. Must dispose properly all the waste chemical used.

III. Avoid hands contact with face, mouth, eyes, and body while using chemical and lab equipment. Repeatedly wash hands with soap after finishing the experiment.

IV. Always use appropriate laboratory equipment when handling chemicals and never use them with your finger because all chemicals in the laboratory are considered hazardous.

V. Immediately rinse with running water for at least 20 minutes if the chemical splash in the eye.

VI. Experiments should be monitored during the reaction or during heating and during observation, keep at least 1 foot away from the specimen.

CHAPTER 4

RESULTS AND DISCUSSION

4.1 Overview

This chapter will show the outcome of this research, explain the results obtain and discuss for further improvement. Besides, this chapter will discuss the comparison of the parameter of the samples including the structure, temperature, and efficiency of the final product. Problems and theories related to this research will be studied in this chapter.

4.2 Results

4.2.1 Chitosan characteristic

4.2.1.1 X-ray Diffraction Spectroscopy (XRD)

Crystalline materials are characterized by a powerful nondestructive technique, X-ray diffraction (XRD). All structures, phases, and preferred crystal (texture) orientations and other structural data are present as well, such as average grain size and crystallinity, strain, and crystal defects. X-ray diffraction peaks are caused by the construction of a monochromatic X-ray beam from every pair of planes of grids in a material distributed at specific angles. The maximum intensities are determined by the atomic distribution in the grid [38]. XRD plot graph is a specific pattern of X-ray intensity versus scattering angle produced in each material.

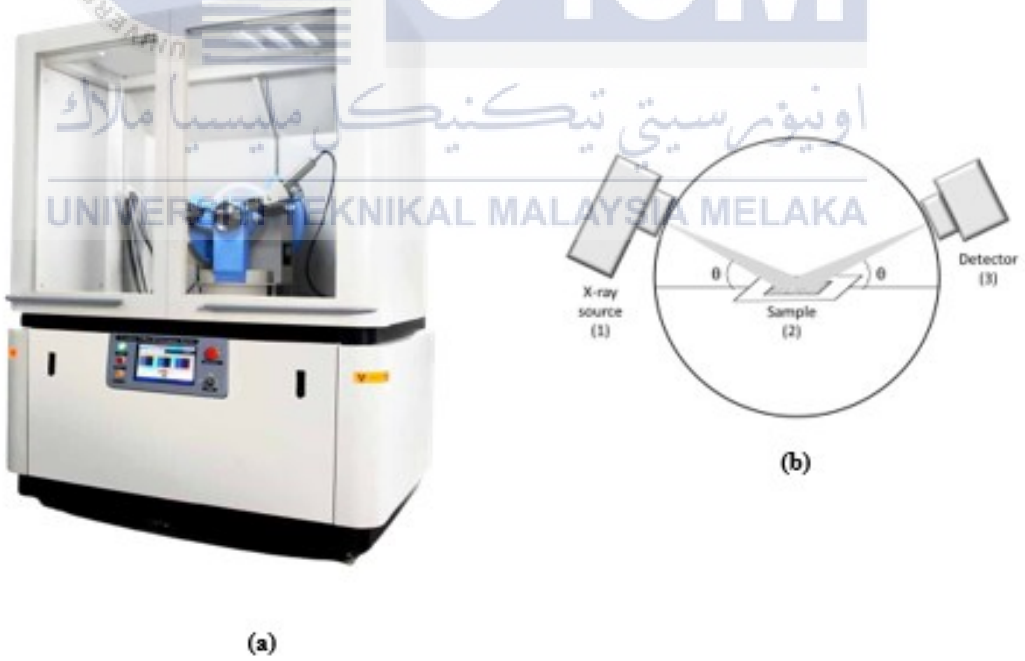

.

Figure 4.1: (a) XRD machine. (b) Work mechanism of XRD

Figure 4.2 show the analyzed spectrum of synthesis chitosan. This results were analyzed by showing all the peaks present at the 2 theta values between 5° and 80°. *Table 4.1* show the maximum peak value for all synthesis chitosan at its respective degree value.

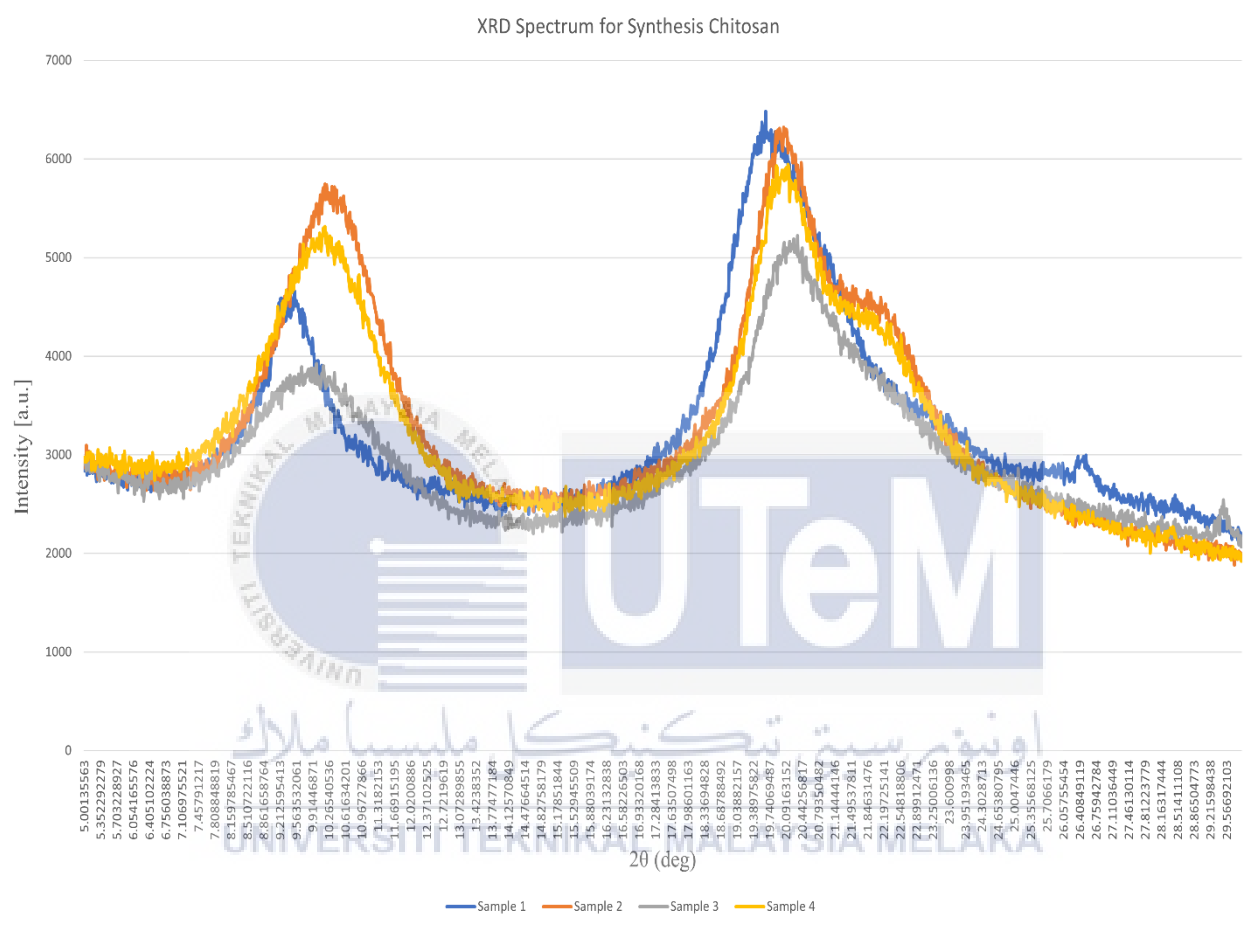

Figure 4.2: XRD pattern of four synthesis chitosan

Table 4.1: Maximum peak value of four synthesis chitosan

Sample	2θ (deg)	Intensity [a.u.]
Sample 1	9.5994	4789.52
	19.5994	6429.17
Sample 2	10.2257	5872.38
	19.9847	6294.75
Sample 3	9.9980	3923.14
	20.2828	5222.01
Sample 4	9.8156	5394.08
	19.8148	5989.25

Spectra pattern in *Figure 4.2* were being compared with to know whether which synthesis chitosan exhibit the supposedly nature. The synthesis of chitosan contains four important step which are drying process, demineralized process, deproteinized process and deacetylation process. The amount of soaking time during deproteinized and deacetylation process affect the quality of chitosan.

4.2.1.2 Scanning Electron Microscope (SEM)

Electron microscopy is mainly divided into two parts, which are Transmission Electron Microscopy (TEM) which study about the inner structure of the sample and Scanning Electron Microscopy (SEM) that function to visualize object's surface. SEM was a microscope device that uses electrons instead of light and photon particles [39].

Figure 4.3: Scanning electron microscope machine

Images of the scanning electron microscope (SEM) for commercial chitosan were shown in *Figure 4.5* with different magnification factor which are magnified by

15x, 30x, and 10Kx. The diameter of particle of the chitosan were measured in micrometer indicate that the chitosan was in micron size. From the image, it is observed that the shape of the particle is like pallet shape. *Figure 4.4*, *Figure 4.5*, *Figure 4.6*, and *Figure 4.7* shows the size of synthesis chitosan particle which can be observed its shape and size. The shape of the particle can be observed to be the almost identical for all the sample chitosan which is pallet like shape. Further magnified show a surface which cannot be defined since the particle sizing is only in micron.

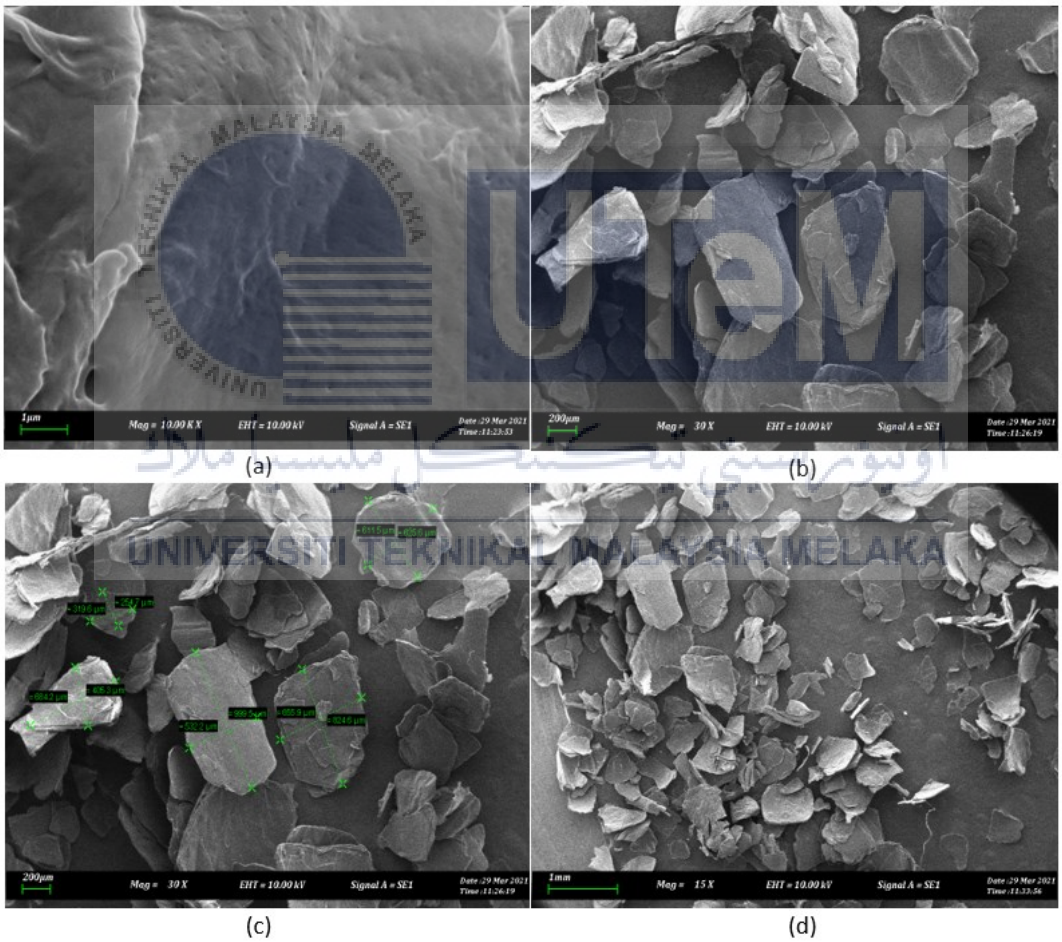

Figure 4.4: SEM images structure of sample 1 chitosan (a) Mag: x10K, (b) Mag: x30, (c) Mag: x30 with diameter of the particle, (d) Mag: x15

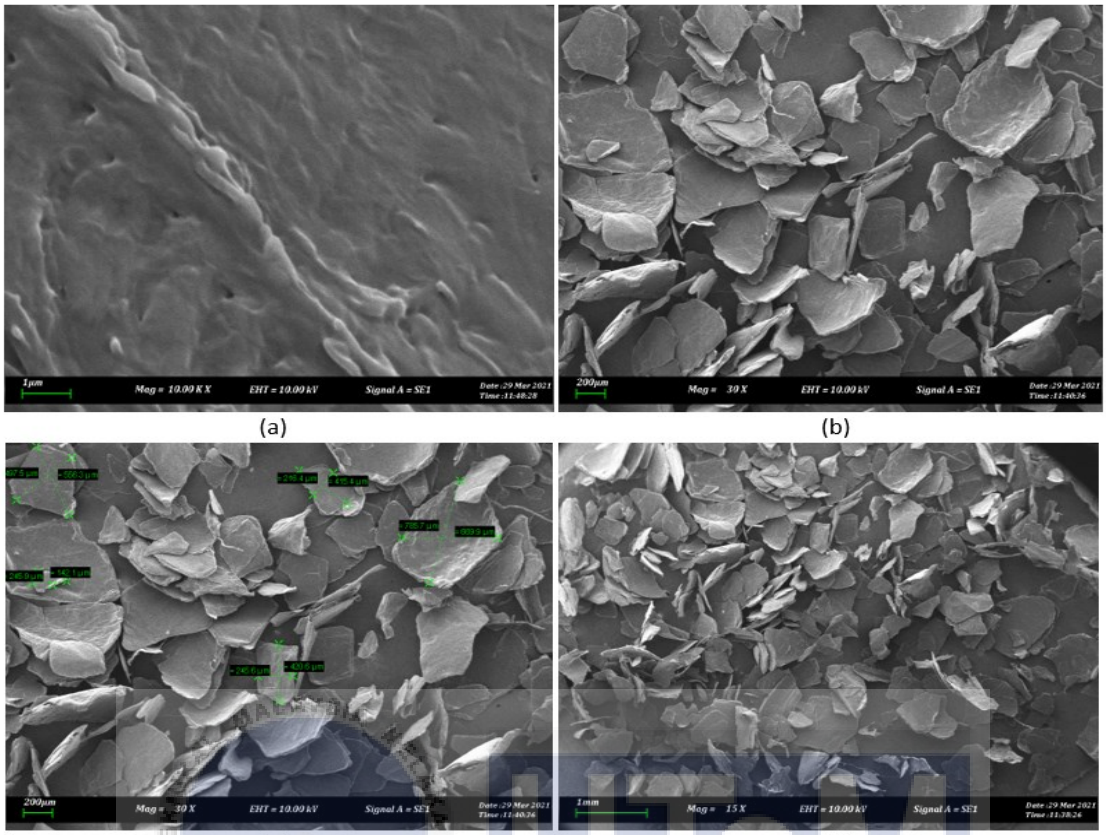

Figure 4.5: SEM images structure of sample 2 chitosan (a) Mag: x10K, (b) Mag: x30, (c) Mag: x30 with diameter of the particle, (d) Mag: x15

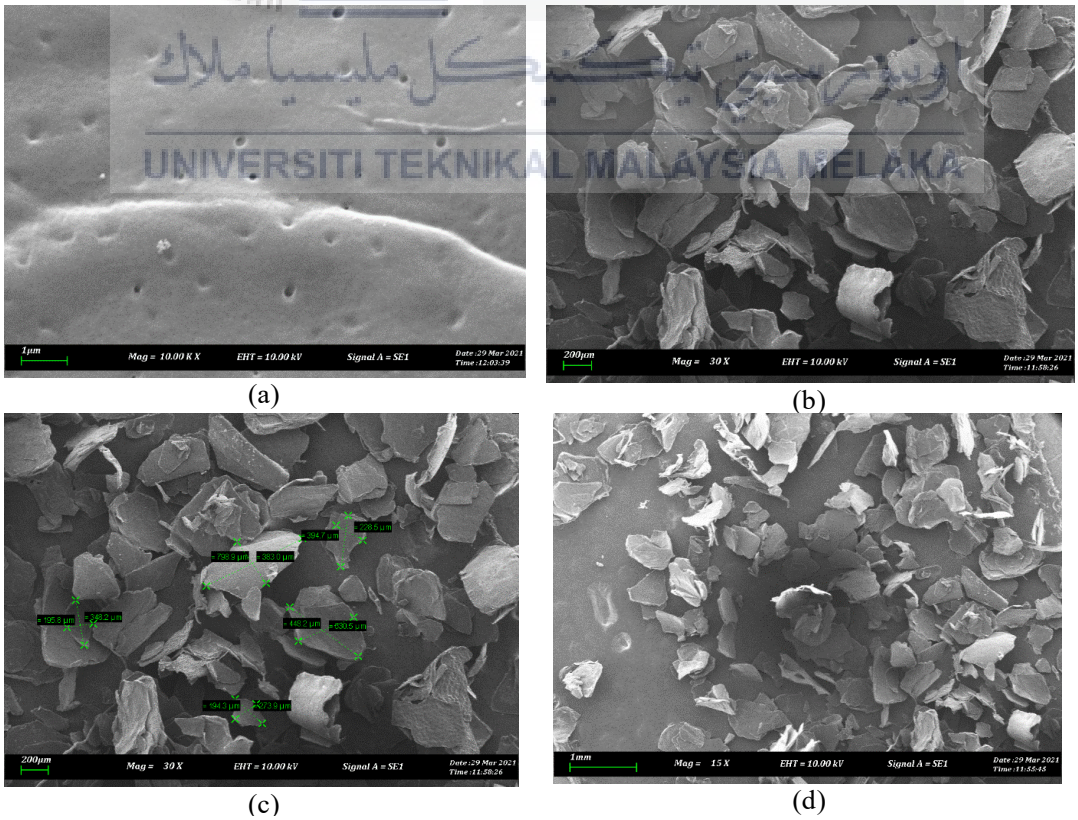

Figure 4.6: SEM images structure of sample 3 chitosan (a) Mag: x10K, (b) Mag: x30, (c) Mag: x30 with diameter of the particle, (d) Mag: x15

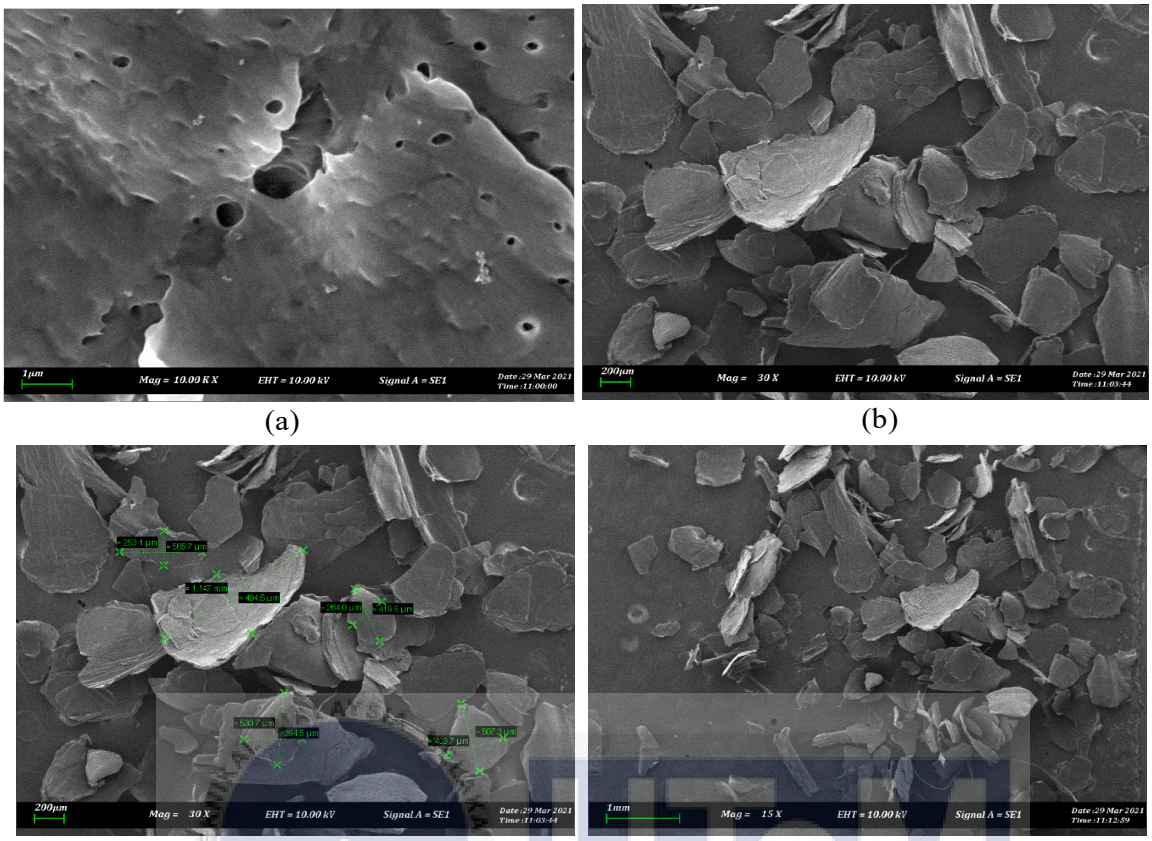

(a) (b)

(c) (d)

Figure 4.7: SEM images structure of sample 4 chitosan (a) Mag: x10K, (b) Mag: x30, (c) Mag: x30 with diameter of the particle, (d) Mag: x15

4.2.1.3 Fourier-transform Infrared Spectroscopy

In order to determine all organic components, including chemical bonds and organic content, simultaneously the Fourier Transform infrared technique (FTIR) was developed. This sort of analysis can be used to characterize liquids, solutions, pastes, powders, films, fibers, and gases, among other substances. This characterization test is relatively quick, accurate, and sensitive [40].

Figure 4.8: Fourier-transform infrared spectroscopy machine

Figure 4.9 shown the FTIR chitosan spectrum for sample 1, sample 2, sample 3, and sample 4 together with its derivatives. The relative peaks for sample 1 chitosan can be seen in the FTIR spectrum. First, a strong and broad extending O-H peak with N-H peak at 3,369 cm^{-1}. Second, C-H is depicted at 2869 cm^{-1} at peak axial expansion. The C=O stretch (amide I), N-H bending (amide II), and C-N stretching (amide III) corresponded to three types of amide chitosan groups, which are described with 1651 cm^{-1}, 1483 cm^{-1} and 1371 cm^{-1}, respectively. The peaks of 1,024 cm^{-1} are the extended oscillation of the skeleton C-O-C [41][42].

For sample 2, the O-H and N-H peak can be seen at 3345 cm^{-1}. The C-H is depicted at 2876 cm^{-1}, peak axial expansion. The three types of amides chitosan groups were spotted at 1661 cm^{-1}, 1503 cm^{-1} and 1379 cm^{-1}, respectively. The extended oscillation of the skeleton C-O-C's peak was at 1031 cm^{-1}. Sample 3 spectrum can be seen to be almost identical with a bit of differences at certain reflectance.

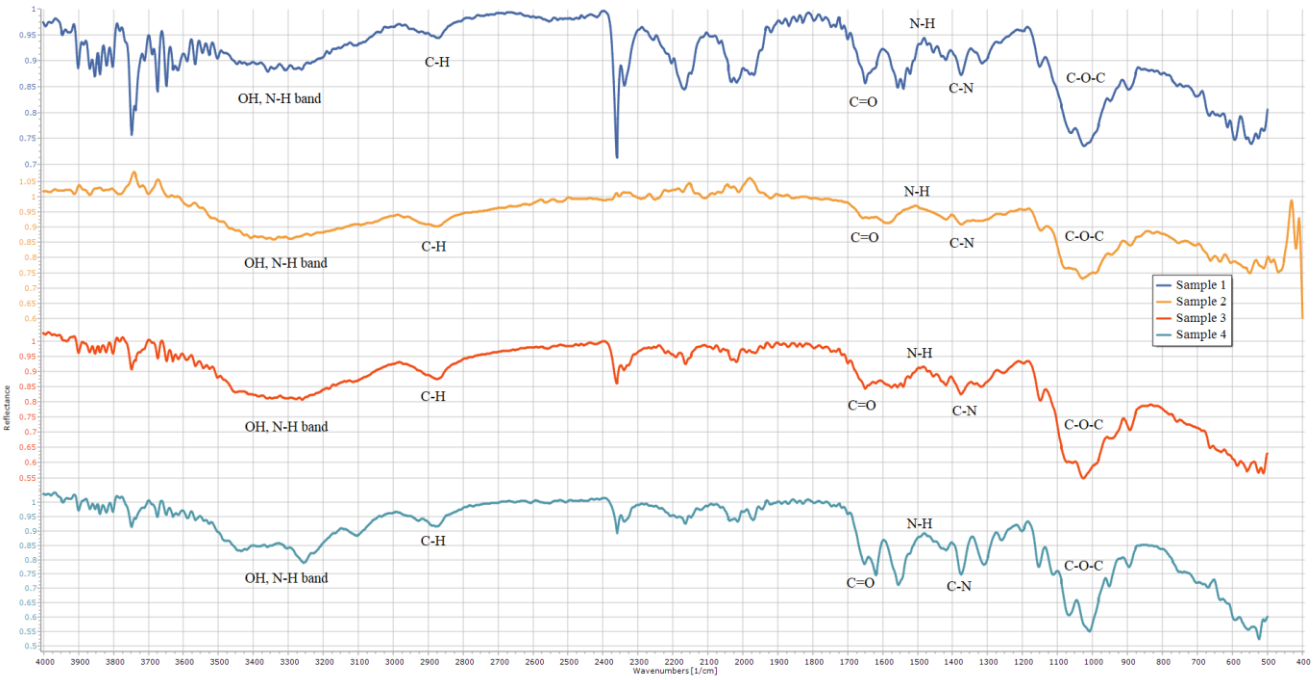

Figure 4.9: FTIR graph pattern of sample 1, 2, 3, and 4

The FTIR spectra for sample 4 can be seen with the broad peak of the spectrum at 3256 cm^{-1}, appoint to the vibrant frequencies N-H and O-H. The highest intensity peak is also assigned to the asymmetric mode in the C-H area of the FTIR spectrum at 2878 cm^{-1}. The spectrum showed an amide bonding peak and the amide bond C=O at 1651 cm^{-1} was observed. High N-H bending vibration of secondary amid was assigned to the peaks at 1483 cm^{-1}. At the top of 1374 cm^{-1}, the last amide is shown as C-N. The peaks at 1010 cm^{-1} correspond to C-O-C skeleton's spread vibration [41][42].

4.2.1.4 Degree of Deacetylation

Degree of deacetylation for each were calculated using *Equation 1*. *Table 4.2* shows the calculated degree of deacetylation for each sample.

Table 4.2: Degree of Deacetylation of Chitosan

Samples	De Queiroz Antonino, R. [33]	Sample 1	Sample 2	Sample 3	Sample 4
Degree of Deacetylation(%)	90%	73%	78%	77%	70%

From *Table 4.2*, the original reference method of synthesis chitosan obtains a high percentage degree of deacetylation of 90%, which can be classified as high-quality chitosan [43]. Sample 1, sample 2, sample 3, and sample 4 obtains the middle degree of deacetylation of 73%, 78%, 77%, and 70%, respectively [43]. Sample 2 achieve the highest degree of deacetylation of 78% of all the samples and can be conclude the best synthesis chitosan to be use for the solar cell fabrication.

4.2.1.5 Percent Error

Percent error was calculated to know the difference between the reference and the experimental obtained degree of deacetylation value. Each samples were compared with the degree of deacetylation obtain from De Queiroz Antonino, R. [33].

Table 4.3: Percent error for each experimental chitosan

Samples	Sample 1	Sample 2	Sample 3	Sample 4
Percent error(%)	18.9%	13.3%	14.4%	22.2%

From Table 4.3, sample 2 shows the lowest percent error while sample 4 shows the highest percent error when being bracket together with the degree of deacetylation from De Queiroz Antonino, R. [33].

4.2.2 Electrical Performance

4.2.2.1 I-V Characteristics of 6% Chitosan-ZnO

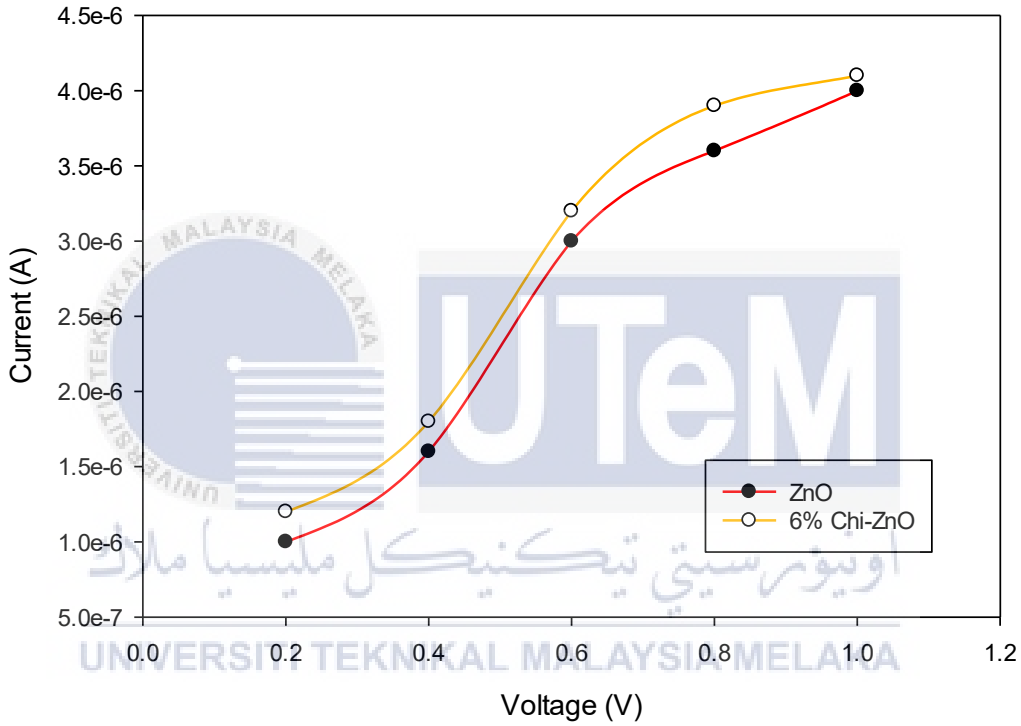

Figure 4.10: I-V measurement comparison between ZnO thin film and 6 % Chi-ZnO thin film

The voltage is supplied between the range of 0.2V to 1V. From figure 4.10, it was shown the increasing of current for both thin film with the increase of voltage supply and the obtain current value was in microampere. The 6% Chi-ZnO thin film show a slightly increase of current value than ZnO thin film. The current value may vary with the increasing of Chi-ZnO thin films concentrations.

4.2.2.2 Electrical Properties

In this process, the current and voltage was measured by using a multimeter. Firstly, voltage performance was measured, the positive probe was inserted in V-port and the negative probe was inserted in COM port of the multimeter. Then, the positive and negative probe is connected to the full assembly DSSC samples. Secondly, the current performance was measured by inserting the positive probe in $20A_{MAX}$ and the negative probe into COM port on the multimeter. Then, both probe is connected to the full assembly DSSC samples. *Table 4.4* showed the measured voltage and current for both samples when bath under the sun.

Table 4.4: Measured voltage and current between ZnO thin film and 6% Chi-ZnO thin film

Sample	Measured Voltage (V)	Measured Current (μA)
ZnO thin film	0.2658	0.2352
6% Chi-ZnO thin film	0.2783	0.2519

Based on *Table 4.4*, there were a slight increase of measured voltage and current of 6% Chi-ZnO thin film than ZnO thin film. There is little significant change between both thin film, but it is hardly to be said that Chi-ZnO thin film word is superior to ZnO thin film.

4.3 GPVDM simulation

4.3.1 Performance of the Organic Solar Cell

All of the simulation use Sun as the light source with similar layer of materials such as ITO as the contact material, Ruthenium as the dye layer, and NiO as the photocathode or bottom layer of the solar cell. *Table 4.5* shows the performance for each type of organic solar cell.

Table 4.5: Performance of the simulated organic solar cell

Type of layer	V_{oc}, (V)	J_{sc}, (Am^{-2})	Fill Factor, (a.u.)	Efficiency, (%)
ZnO layer	0.7056	-64.9106	0.7698	3.0947
ZnO+100nm thickness Chitosan layer	0.6950	-45.9030	0.7698	2.2302
ZnO+120nm thickness Chitosan layer	0.6956	-53.3587	0.7521	2.5456
ZnO+140nm thickness Chitosan layer	0.6941	-57.8242	0.7426	2.7070
ZnO+160nm thickness Chitosan layer	0.6917	-60.3839	0.7297	2.7645
ZnO+180nm thickness Chitosan layer	0.6928	-58.0733	0.7367	2.7363
ZnO+200nm thickness Chitosan layer	0.6950	-54.9131	0.7478	2.6436

Based on *Figure 4.11*, each simulation sample exhibit almost the same I-V curve as the fill factor value shown for all the simulation has a small differences with average fill factor of 0.7497 a.u..

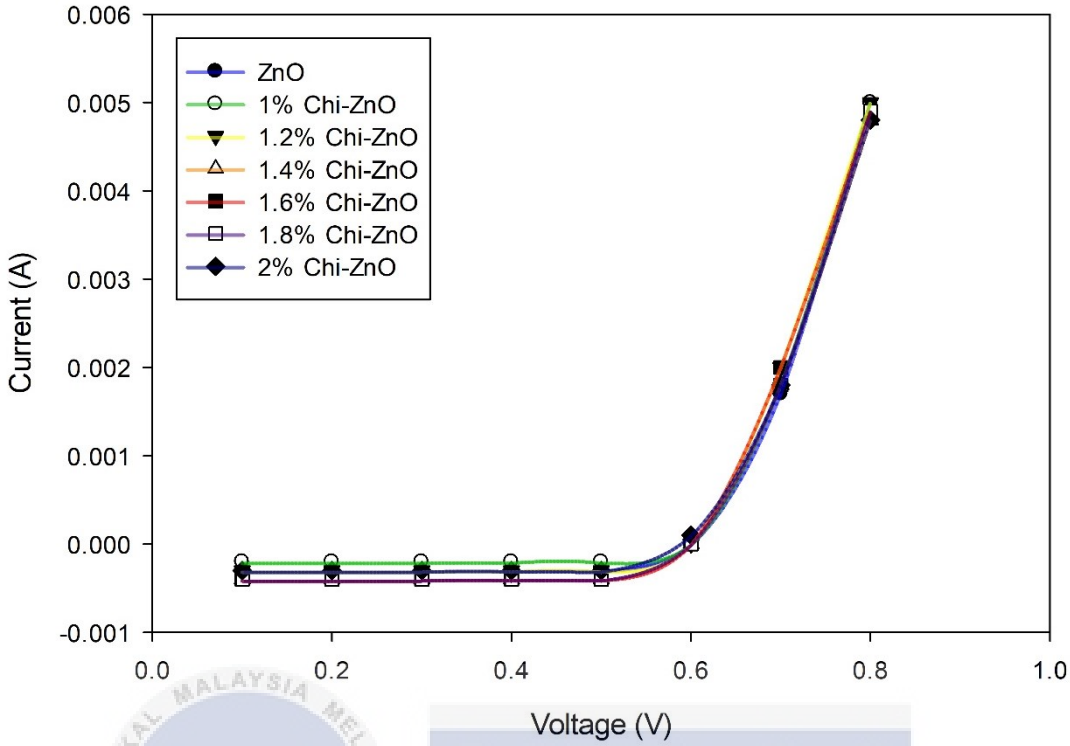

Figure 4.11: Simulation I-V graph

Table 4.6: Electron generation rate for each devices

Type	Generation rate
ZnO layer	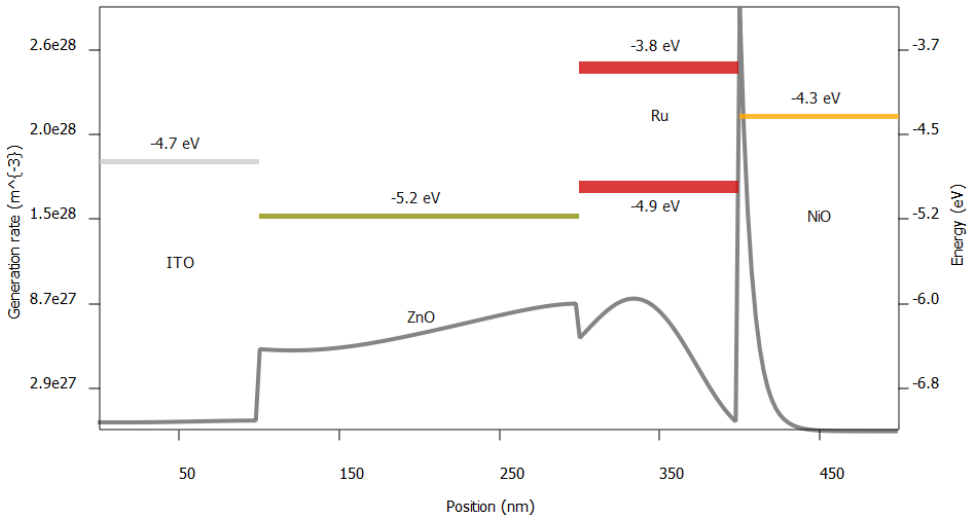

ZnO+100nm thickness Chitosan layer	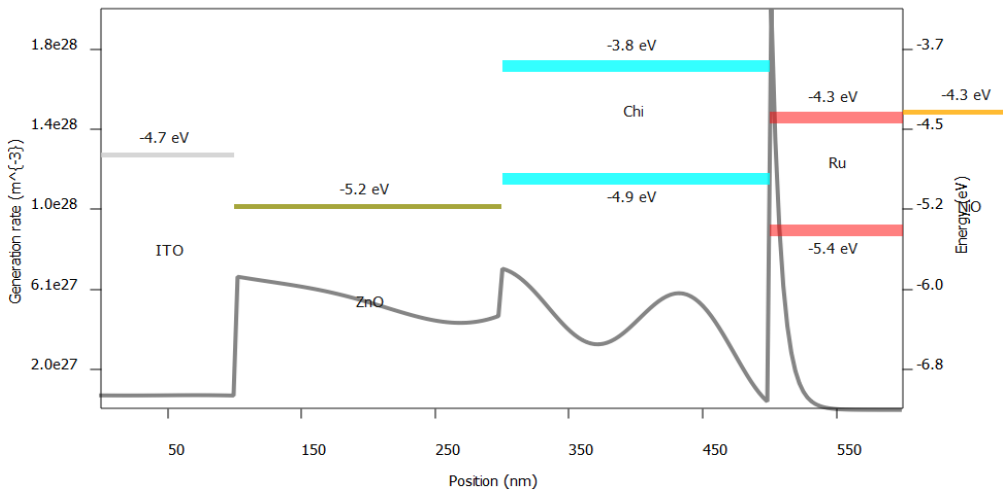
ZnO+120nm thickness Chitosan layer	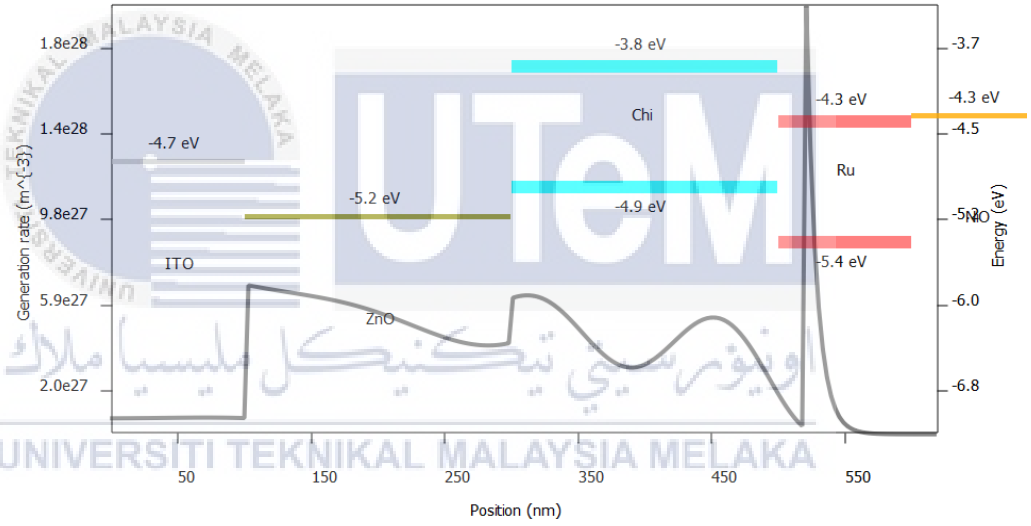
ZnO+140nm thickness Chitosan layer	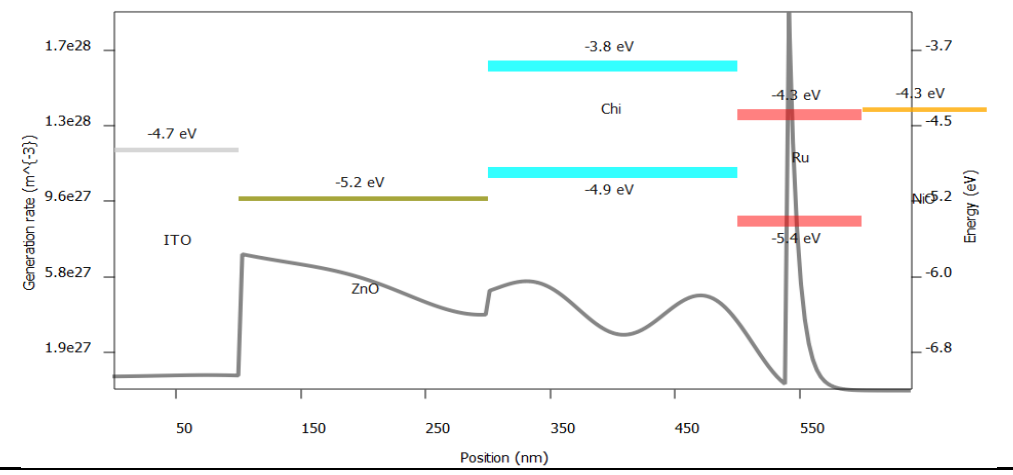

ZnO+160nm thickness Chitosan layer	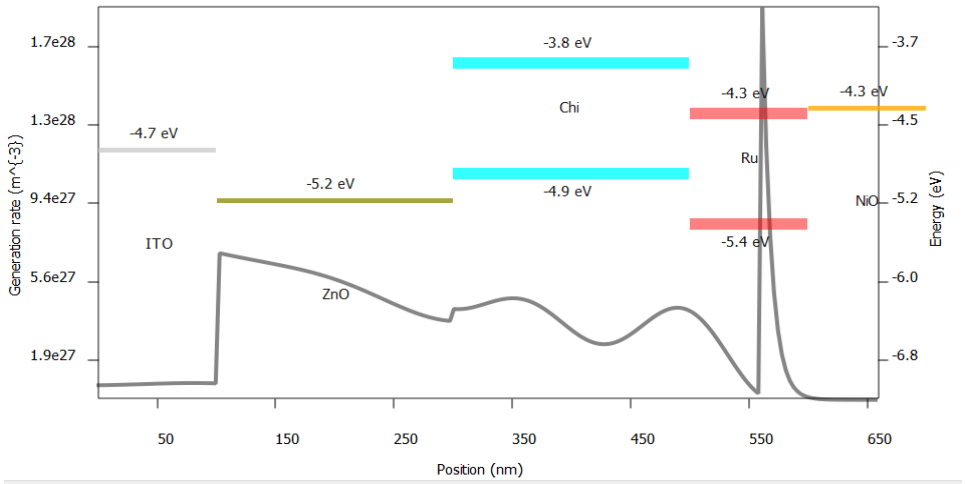
ZnO+180nm thickness Chitosan layer	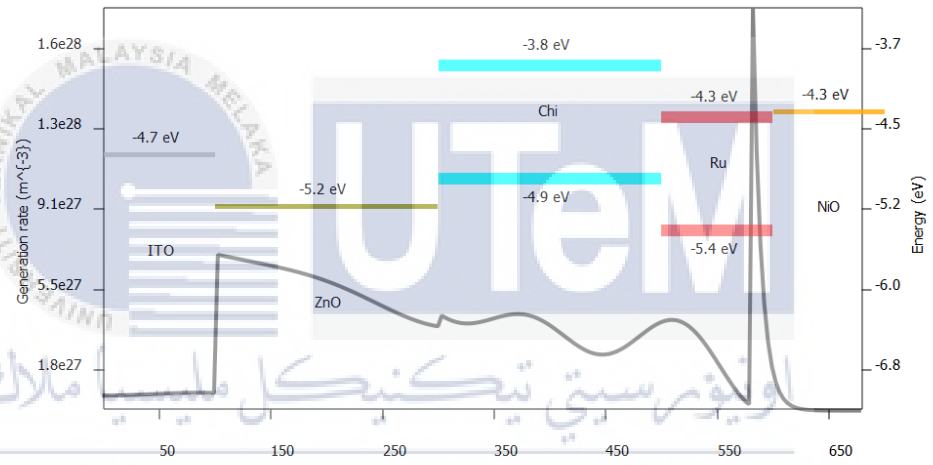
ZnO+200nm thickness Chitosan layer	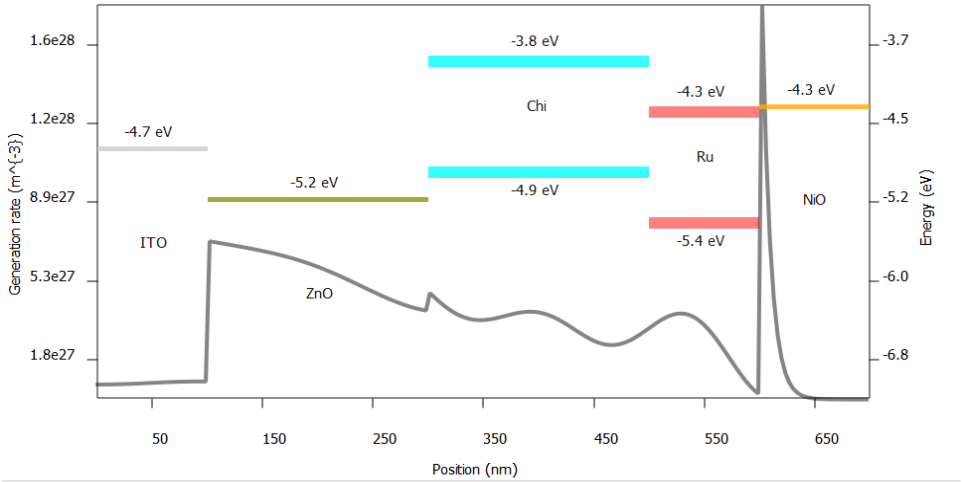

Table 4.6 show the generation rate of electron at every position in the multilayer devices. ZnO layer device exhibit a high electron generation rate at the Ru position with 8.7e27 m^{-3}. For ZnO+100nm thickness chitosan layer, the highest rate can be seen at the boundary between chitosan and ZnO layer with more than 6.1e27 m^{-3}. For the rest, the generation rate only peak in between ZnO and ITO contact glass with the generation rate of 5.9e27 m^{-3}, 5.8e27 m^{-3}, 5.6e27 m^{-3}, 5.5e27 m^{-3}, and 5.3e27 m^{-3}, respectively.

Table 4.7: Photon density in the devices

Type	Photon density
ZnO layer	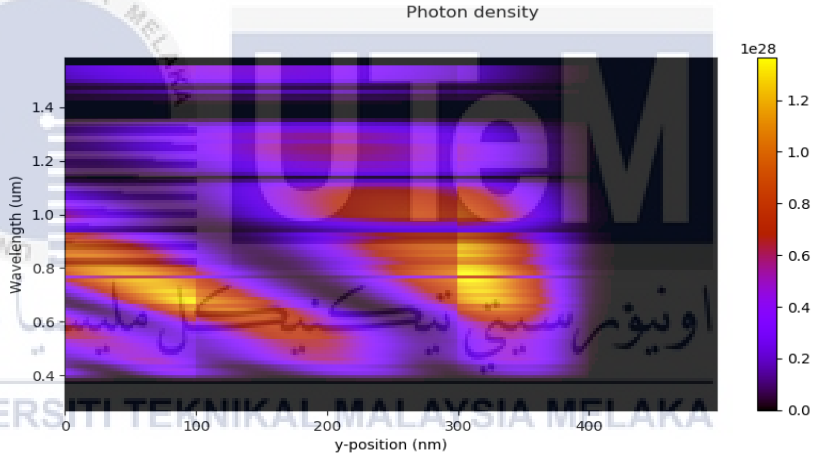
ZnO+100nm thickness Chitosan layer	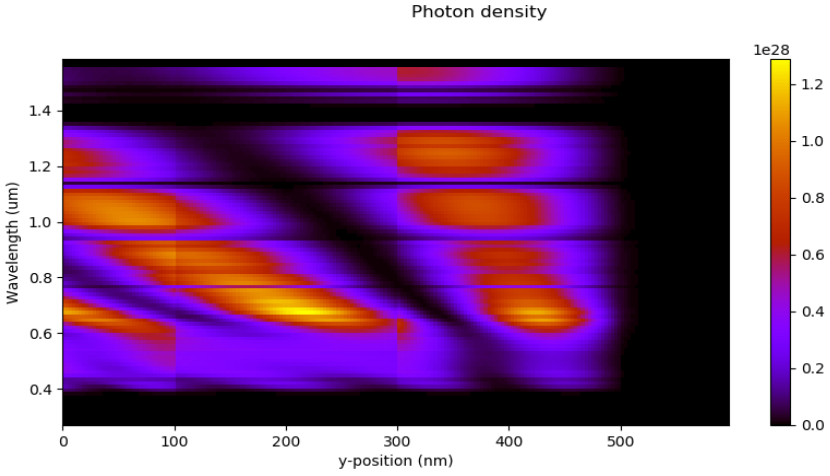

ZnO+120nm thickness Chitosan layer	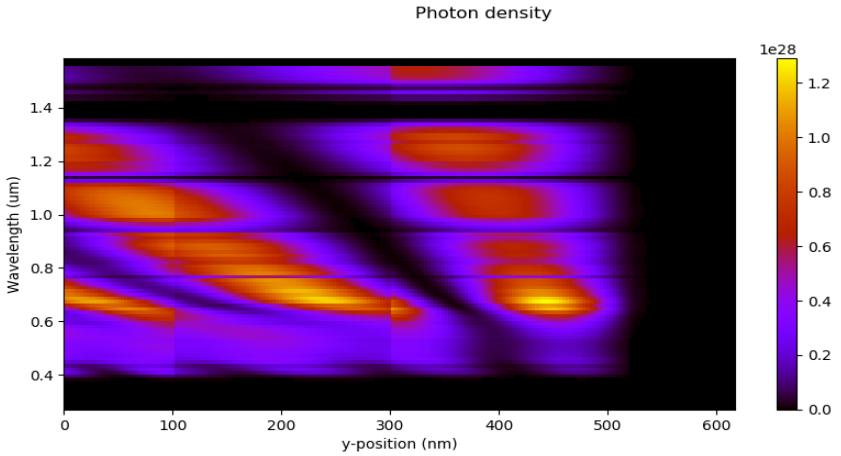
ZnO+140nm thickness Chitosan layer	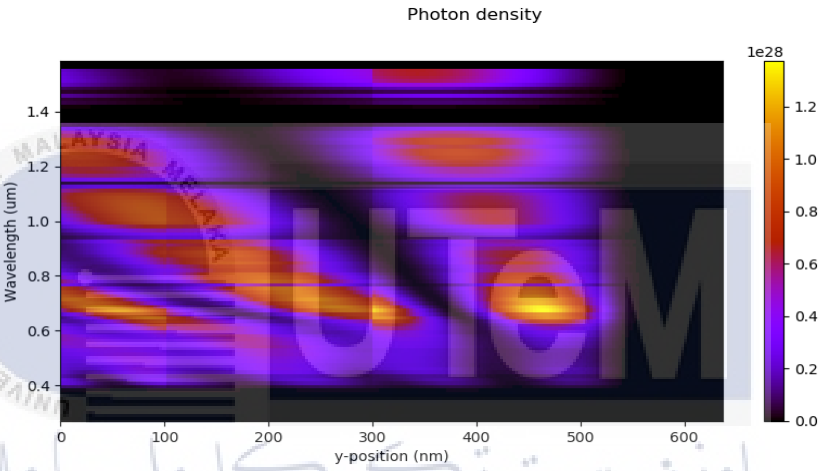
ZnO+160nm thickness Chitosan layer	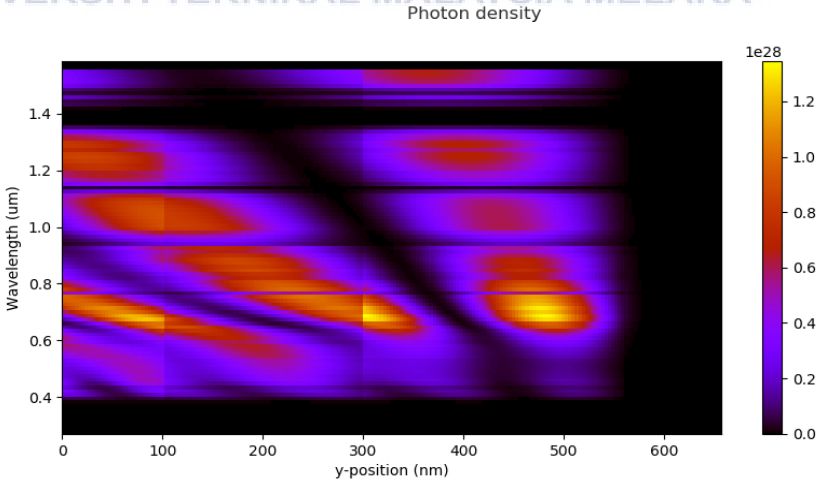

ZnO+180nm thickness Chitosan layer	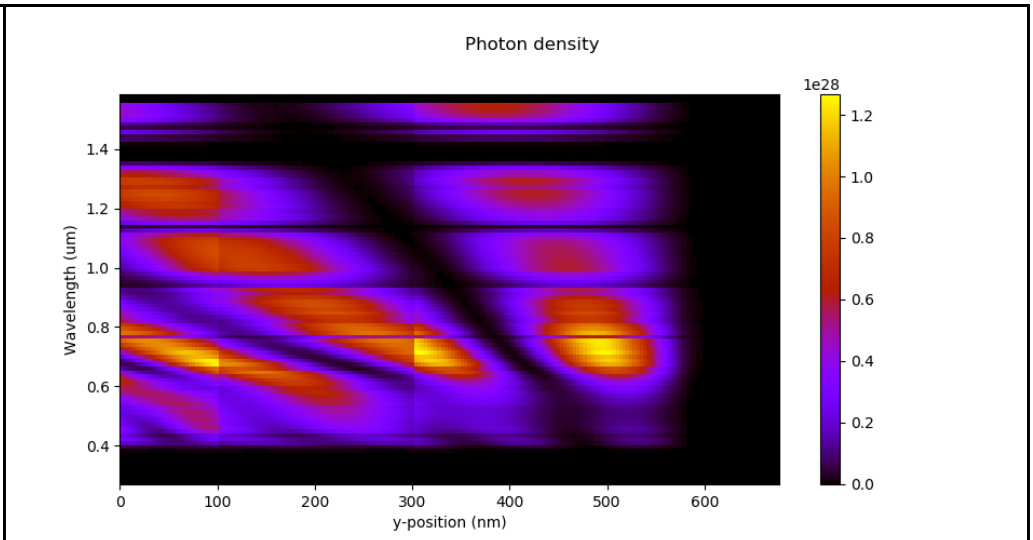
ZnO+200nm thickness Chitosan layer	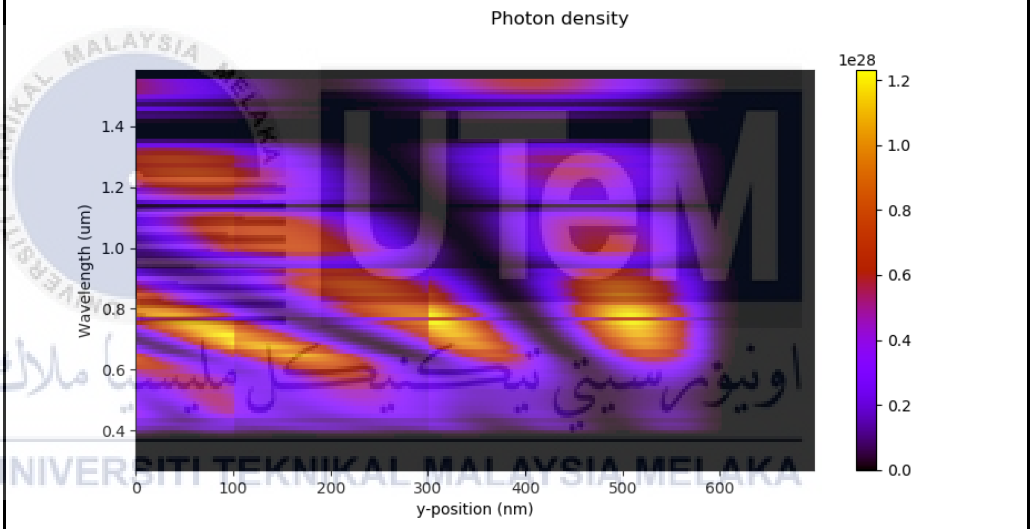

Table 4.7 shows the photon density at each y-position which means the positioning of material in the devices. The ZnO layer shows a bright red at position 200nm to 300 nm as it is supposedly to be the position of Ru. The rest of the device exhibit a high photon density at y-position of 400nm to 500nm.

4.4 Discussion

4.4.1 Chitosan

During Chitosan synthesis, the dried shrimp shell needs to be crush as fined as possible reaching nanoparticles size. Nanoparticle size Chitosan were easier to diluted into solution compared to micron particle size Chitosan. From several experiment to synthesis Chitosan, the soaking time period during deproteinization and deacetylation process affect the chemical bond of the end product Chitosan. The longer the soaking time, a preferred Chitosan can be synthesis.

4.4.2 Spin coating technique

During ZnO paste depositing, the duration and speed of the machine needs to be adjusted according to the thickness of solution. The thicker the solution, the longer the duration and the faster the speed of the spin coating machine. Besides that, after every deposition, the base, and the area around it need to be clean using ethanol to prevent contamination.

4.4.3 Annealing

During the annealing process, the plastic side is important as we must ensure that the ITO plastic is placed face up and ordinary plastic face down on the hot plate surface. This is because if we misplaced the side, the ITO in the plastic might be burned and melted, at the same time can affect the ITO structure. Moreover, the annealing time also important as the time takes for annealing is too short, the paste will not fully be attached to the ITO plastic and the time take for annealing should not cost more than an hour.

4.4.4 Fabrication process

After a few dye drops are poured on the ITO side, it needs to leave for a while to allow the dye to absorb into the annealed layer of ZnO. The longer it leaves, the higher dye will absorb toward the ZnO layer. During dye, the dye should be drop between the ZnO pastes so it can spread smoothly through the paste. This is to avoid the ZnO paste from detached due to the pressure from the dye. The full assembly solar cell is exposed under the scorching hot sun to ensure that it obtained the maximum energy from the photon

4.4.5 X-ray Diffraction Spectroscopy (XRD)

Two crystalline peaks are shown approximately at 10° and 20° in *Figure 4.2*. XRD analyses have been applied for native and linked chitosan crystallinity characterization [44]. The first peak at 10°(2θ) represent the first crystalline while the peak at 20°(2θ) represent the second crystalline of the chitosan. The differences of intensity [a.u.] value between both XRD pattern is due to the moisture of the sample during machine testing. If the moisture in the synthesis sample is low, the intensity [a.u.] value can approximately match the commercial sample intensity [a.u.] value.

4.4.6 Scanning Electron Microscope (SEM)

Electron Microscope is a scientific instrument whose function is to analyze objects at a very small scale with a highly energetic electron beam. This analysis can gain details about the composition, morphology, topography, and crystallography. The topography is an object's surface feature like hardness and reflectivity, while morphology refers to particle shape and size such as flexibility, solidity, and shape. Next, the composition's information is about the elements and compounds that the object is produced and their relative quantity. In the meantime, crystallographic detail

is about how the object's atoms are organized.

SEM is also a powerful tool as it can characterize an extensive specimen from nanometer to micrometer length scale due to its high spatial resolution. SEM image does not have any color as it does not use any light, and the only thing it can do is figure out what surface of the sample.

4.4.7 Fourier-transform Infrared Spectroscopy (FTIR)

Fourier-transform Infrared Spectroscopy is a technique for the obtaining of a solid, liquid and gas infrared spectrum of absorption or emission. The functional groups present in the chitosan were evaluated using the FTIR test. From the FTIR spectrum, the data needed to calculate the degree of deacetylation can be found. The calculated degree of deacetylation exhibit that sample 2 was the most successful chitosan that have been synthesis with 78% degree of deacetylation and 13.3% percent error.

4.4.8 Electrical Properties

The voltage and current were measured using a normal battery powered multimeter which its accuracy is not precise, and the measured value can be doubt. If the DSSC device have been measured using digital multimer where its accuracy is certain and has confidence with the measured value obtained.

4.4.9 GPVDM Simulation

GPVDM simulation works by putting the desired layer in accordance and change the electrical parameter of the material used. *Table 4.5* show the output information of the device. From the efficiency obtain, ZnO only layer shows the highest efficiency that any of the Chitosan-ZnO layer with 3.0947%. ZnO with 160nm

thickness Chitosan layer shows the highest efficiency from other mix layer with 2.7645%. This shows that Chitosan does not improve the efficiency of dye-sensitized solar cell with the current used parameter and material.

CHAPTER 5

CONCLUSION AND FUTURE WORKS

5.1 Conclusion

Dye-Sensitized Solar Cell (DSSC) is one of the solar cell in the third generation alongside Perovskite with tremendous potential in the renewable energy industry for the future healthier environment. This is because DSSC is a non-toxic solar cell as the silicon solar cell, and it can use natural dye only to absorb photons from sunlight to the photoanode layer. In this project, chitosan was successfully synthesis from shrimp shell. From personal observation, different time period taken for soaking the shrimp shell during deproteinization and deacetylation gave out different output as chitosan. The longer the shrimp shell soaking time, the better the resulted chitosan. The synthesis chitosan was characterized and analyzed using Scanning Electron Microscope (SEM), X-ray Diffraction Spectroscopy (XRD) and Fourier-transform Infrared Spectroscopy (FTIR). All the results for the synthesis

chitosan were compared with each other to know which are the highest quality chitosan have been synthesis.

For the fabrication process, natural dye was used replacing standard dye, Ru (II) polypyridyl or N719 dye. The natural dye was accomplished using blueberries as the main component of the dye. Beside dye, the electrolyte used was potassium bromide, KBr which also a strong electrolyte as potassium iodide, KI. The ZnO Thin Film is deposited with spin-coating technology on indium tin oxide (ITO) glass and rinsed for 10 minutes at 60°C. For the photocathode substrate, Graphene Oxide (GO) were use and being deposited on ITO using spin coating technique. The full assembly DSSC was tested under sunlight by measuring the current using multimeter.

Using GPVDM simulation, the functionality of chitosan can be seen theoretically. All device that contains chitosan layer did not accomplish efficiency as high as the ZnO layer only device. On the other hand, different thickness of chitosan in the device resulting different output value for efficiency, fill factor, V_{oc}, and J_{sc}.

5.2 Future Works

For future works, this project showed an ability that can further improve the technology of dye-sensitized solar cell. The quality of chitosan can be further enhanced to be more compatible with metal using an improvise synthesis method. The thickness factor can be studied in future work by using another method. There are many improvement can be made to increase the efficiency of dye-sensitized solar cell, from the quality of material used, a better synthesis dye solution used, a stronger redox solution, and the handling process during the production. The use of chitosan as can embedded in another component of the dye-sensitized solar cell. For example, using chitosan as a dye, redox solution or in the counter electrode.

REFERENCES

[1] K. Ranabhat, L. Patrikeev, A. A. evna Revina, K. Andrianov, V. Lapshinsky, and E. Sofronova, "An introduction to solar cell technology," *J. Appl. Eng. Sci.*, 2016, doi: 10.5937/jaes14-10879.

[2] G. Ali, M. Omar, A. K. Khan, and M. Faisal Nadeem, "Recent Challenges of Solar Cell Technologies; A Critical Analysis," *RAEE 2018 - Int. Symp. Recent Adv. Electr. Eng.*, pp. 1–5, 2018, doi: 10.1109/RAEE.2018.8706887.

[3] M. B. Tahir, M. Abrar, A. Tehseen, T. I. Awan, A. Bashir, and G. Nabi, *Nanotechnology: the road ahead*. INC, 2020.

[4] M. Mazalan, M. M. Noh, Y. Wahab, M. N. Norizan, and I. S. Mohamad, "Development of dye-sensitized solar cell (DSSC) using patterned indium tin oxide (ITO) glass: Fabrication and testing of DSSC," *CEAT 2013 - 2013 IEEE Conf. Clean Energy Technol.*, no. January 2016, pp. 187–191, 2013, doi: 10.1109/CEAT.2013.6775624.

[5] N. G. Park, "Perovskite solar cells: An emerging photovoltaic technology," *Materials Today*. 2015, doi: 10.1016/j.mattod.2014.07.007.

[6] M. A. Green, E. D. Dunlop, D. H. Levi, J. Hohl-Ebinger, M. Yoshita, and A. W. Y. Ho-Baillie, "Solar cell efficiency tables (version 54)," *Prog. Photovoltaics Res. Appl.*, 2019, doi: 10.1002/pip.3171.

[7] S. Shalini, R. Balasundaraprabhu, T. Satish Kumar, N. Prabavathy, S. Senthilarasu, and S. Prasanna, "Status and outlook of sensitizers/dyes used in dye sensitized solar cells (DSSC): a review," *International Journal of Energy Research*. 2016, doi: 10.1002/er.3538.

[8] P. Chawla, A. Srivastava, and M. Tripathi, "Performance of chitosan based polymer electrolyte for natural dye sensitized solar cell," *Environ. Prog. Sustain. Energy*, vol. 38, no. 2, pp. 630–634, 2019, doi: 10.1002/ep.12965.

[9] R. Vittal and K. C. Ho, "Zinc oxide based dye-sensitized solar cells: A review,"

Renew. Sustain. Energy Rev., vol. 70, no. March 2016, pp. 920–935, 2017, doi: 10.1016/j.rser.2016.11.273.

[10] D. Wei, "Dye sensitized solar cells," *Int. J. Mol. Sci.*, vol. 11, no. 3, pp. 1103–1113, 2010, doi: 10.3390/ijms11031103.

[11] S. Shalini, R. Balasundara Prabhu, S. Prasanna, T. K. Mallick, and S. Senthilarasu, "Review on natural dye sensitized solar cells: Operation, materials and methods," *Renewable and Sustainable Energy Reviews*. 2015, doi: 10.1016/j.rser.2015.07.052.

[12] A. Carella, F. Borbone, and R. Centore, "Research progress on photosensitizers for DSSC," *Frontiers in Chemistry*. 2018, doi: 10.3389/fchem.2018.00481.

[13] K. Sharma, V. Sharma, and S. S. Sharma, "Dye-Sensitized Solar Cells: Fundamentals and Current Status," *Nanoscale Research Letters*. 2018, doi: 10.1186/s11671-018-2760-6.

[14] R. A. Afre, N. Sharma, M. Sharon, and M. Sharon, "Transparent conducting oxide films for various applications: A review," *Reviews on Advanced Materials Science*. 2018, doi: 10.1515/rams-2018-0006.

[15] L. Y. Lin and K. C. Ho, "Dye-sensitized solar cells," *Encycl. Mod. Opt.*, vol. 1–5, pp. 270–281, 2018, doi: 10.1016/B978-0-12-803581-8.09545-X.

[16] M. E. Yeoh and K. Y. Chan, "Recent advances in photo-anode for dye-sensitized solar cells: a review," *Int. J. Energy Res.*, vol. 41, no. 15, pp. 2446–2467, 2017, doi: 10.1002/er.3764.

[17] M. Ye *et al.*, "Recent advances in dye-sensitized solar cells: From photoanodes, sensitizers and electrolytes to counter electrodes," *Mater. Today*, vol. 18, no. 3, pp. 155–162, 2015, doi: 10.1016/j.mattod.2014.09.001.

[18] N. T. R. N. Kumara, A. Lim, C. M. Lim, M. I. Petra, and P. Ekanayake, "Recent progress and utilization of natural pigments in dye sensitized solar cells: A review," *Renewable and Sustainable Energy Reviews*. 2017, doi: 10.1016/j.rser.2017.04.075.

[19] A. Omar and H. Abdullah, "Electron transport analysis in zinc oxide-based dye-sensitized solar cells: A review," *Renewable and Sustainable Energy Reviews*. 2014, doi: 10.1016/j.rser.2013.11.031.

[20] N. Prabavathy, S. Shalini, R. Balasundaraprabhu, D. Velauthapillai, S. Prasanna, and N. Muthukumarasamy, "Enhancement in the photostability of natural dyes for dye-sensitized solar cell (DSSC) applications: a review," *International Journal of Energy Research*. 2017, doi: 10.1002/er.3703.

[21] B. Boro, B. Gogoi, B. M. Rajbongshi, and A. Ramchiary, "Nano-structured TiO2/ZnO nanocomposite for dye-sensitized solar cells application: A review," *Renew. Sustain. Energy Rev.*, vol. 81, no. May, pp. 2264–2270, 2018, doi:

10.1016/j.rser.2017.06.035.

[22] P. P. Kumavat, P. Sonar, and D. S. Dalal, "An overview on basics of organic and dye sensitized solar cells, their mechanism and recent improvements," *Renew. Sustain. Energy Rev.*, vol. 78, no. May, pp. 1262–1287, 2017, doi: 10.1016/j.rser.2017.05.011.

[23] Q. Yang, W. Yang, Y. Zhang, W. Ge, X. Yang, and P. Yang, "Precise surface state control of carbon quantum dots to enhance charge extraction for solar cells," *Nanomaterials*, vol. 10, no. 3, pp. 1–11, 2020, doi: 10.3390/nano10030460.

[24] M. Z. Iqbal, S. R. Ali, and S. Khan, "Progress in dye sensitized solar cell by incorporating natural photosensitizers," *Solar Energy*. 2019, doi: 10.1016/j.solener.2019.02.023.

[25] A. M. Zulkifli *et al.*, "Characteristics of Dye-Sensitized Solar Cell Assembled from Modified Chitosan-Based Gel Polymer Electrolytes Incorporated with Potassium Iodide," *Molecules*, 2020, doi: 10.3390/molecules25184115.

[26] S. Peter, N. Lyczko, D. Gopakumar, H. J. Maria, A. Nzihou, and S. Thomas, "Chitin and Chitosan Based Composites for Energy and Environmental Applications: A Review," *Waste and Biomass Valorization*, no. 0123456789, 2020, doi: 10.1007/s12649-020-01244-6.

[27] Y. Yang, C. Sun, H. L. Yip, R. Sun, and X. Wang, "Chitosan-Assisted Crystallization and Film Forming of Perovskite Crystals through Biomineralization," *Chem. - An Asian J.*, vol. 11, no. 6, pp. 893–899, 2016, doi: 10.1002/asia.201501425.

[28] E. M. Jin *et al.*, "Preparation and characterization of chitosan binder-based TiO 2 electrode for dye-sensitized solar cells," *Int. J. Photoenergy*, vol. 2013, pp. 1–8, 2013, doi: 10.1155/2013/296314.

[29] I. Younes and M. Rinaudo, "Chitin and chitosan preparation from marine sources. Structure, properties and applications," *Marine Drugs*. 2015, doi: 10.3390/md13031133.

[30] M. H. Buraidah, L. P. Teo, and A. K. Arof, "Determining the potential of 55 wt.% chitosan-45 wt.% NH4I biopolymer electrolyte for application in dye-sensitized solar cells," *Mol. Cryst. Liq. Cryst.*, vol. 695, no. 1, pp. 1–9, 2019, doi: 10.1080/15421406.2020.1723900.

[31] E. Praveen, I. J. Peter, A. M. Kumar, K. Ramachandran, and K. Jayakumar, "Boosting of Power Conversion Efficiency of 2D ZnO Nanostructures-Based DSSC by the Lorentz Force with Chitosan Polymer Electrolyte," *J. Inorg. Organomet. Polym. Mater.*, vol. 0123456789, 2020, doi: 10.1007/s10904-020-01629-z.

[32] F. H. Muhammad, R. H. Y. Subban, and T. Winie, "Solid solutions of hexanoyl

chitosan/poly(vinyl chloride) blends and NaI for all-solid-state dye-sensitized solar cells," *Ionics (Kiel).*, 2019, doi: 10.1007/s11581-019-02855-3.

[33] De Queiroz Antonino, R., Lia Fook, B., de Oliveira Lima, V., de Farias Rached, R., Lima, E., da Silva Lima, R., … Lia Fook, M. (2017). *Preparation and Characterization of Chitosan Obtained from Shells of Shrimp (Litopenaeus vannamei Boone). Marine Drugs, 15(5), 141.* doi:10.3390/md15050141

[34] Trung, T. S., Tram, L. H., Van Tan, N., Van Hoa, N., Minh, N. C., Loc, P. T., & Stevens, W. F. (2020). *Improved method for production of chitin and chitosan from shrimp shells. Carbohydrate Research, 107913.* doi:10.1016/j.carres.2020.107913

[35] Prokhorov, E., Luna-Bárcenas, G., Yáñez Limón, J. M., Gómez Sánchez, A., & Kovalenko, Y. (2020). Chitosan-ZnO Nanocomposites Assessed by Dielectric, Mechanical, and Piezoelectric Properties. Polymers, 12(9), 1991. doi:10.3390/polym12091991

[36] Vijayalakshmi, V., HIna Kousar, P. A., & Sukhi Das, (2020). Optimization And Characterization Of Chitosan Based Nanocarrier For The Application Of Cancer Drug Delivery. Journal of Critical Reviews, 7(7), 762-769. doi: 10.31838/jcr.07.07.139

[37] Azofeifa, D. E., Arguedas, H. J., & Vargas, W. E. (2012). Optical properties of chitin and chitosan biopolymers with application to structural color analysis. Optical Materials, 35(2), 175–183. doi:10.1016/j.optmat.2012.07.024

[38] Shimizu, S. S. (2013, April 3). *ZnO bandgap engineering*. Department of Mechanical and Aerospace Engineering Materials Science and Engineering Program . http://maeresearch.ucsd.edu/mckittrick/index_files/Page945.htm.

[39] Hussain, B., Aslam, A., Khan, T., Creighton, M., & Zohuri, B. (2019). Electron Affinity and Bandgap Optimization of Zinc Oxide for Improved Performance of ZnO/Si Heterojunction Solar Cell Using PC1D Simulations. Electronics, 8(2), 238. doi:10.3390/electronics8020238

[40] Akman, F. (2016). Prediction Of Chemical Reactivity Of Cellulose And Chitosan Based On Density Functional Theory. *CELLULOSE CHEMISTRY AND TECHNOLOGY*, *51*(3-4), 253–262. https://www.cellulosechemtechnol.ro/pdf/CCT3-4(2017)/p.253-262.pdf.

[41] Bunaciu, A. A., Udriştioiu, E. gabriela, & Aboul-Enein, H. Y. (2015). X-Ray Diffraction: Instrumentation and Applications. Critical Reviews in Analytical Chemistry, 45(4), 289–299. doi:10.1080/10408347.2014.949616.

[42] W. Zhou, R. Apkarian, Z. L. Wang, and D. Joy, "Fundamentals of scanning electron microscopy (SEM)," *Scanning Microsc. Nanotechnol. Tech. Appl.*, pp. 1–40, 2007, doi: 10.1007/978-0-387-39620-0_1.

[43] Lv, S. H. (2016). High-performance superplasticizer based on chitosan. Biopolymers and Biotech Admixtures for Eco-Efficient Construction Materials, 131–150. doi:10.1016/b978-0-08-100214-8.00007-5

[44] Nandiyanto, A. B. D., Oktiani, R., & Ragadhita, R. (2019). How to Read and Interpret FTIR Spectroscope of Organic Material. *Indonesian Journal of Science & Technology, 4(1)*, 97-118, http://dx.doi.org/10.17509/ijost.v4i1.15806.